

AMERICAN UNIVERSITY OF BEIRUT

ASSESSMENT OF THE PUNCHING SHEAR BEHAVIOR OF
INTERIOR SLAB-COLUMN CONNECTIONS
STRENGTHENED BY HEMP FIBERS SHEET FABRICS

by
LOAI KHALED AL-MAWED

A thesis
Submitted in partial fulfillment of the requirements
for the degree of Master of Engineering
to the Department of Civil and Environmental Engineering
of the Maroun Semaan Faculty of Engineering and Architecture
at the American University of Beirut

Beirut, Lebanon
April 2021

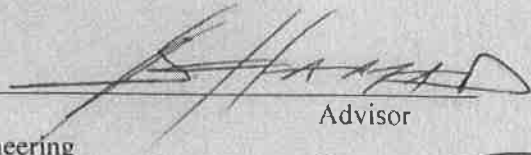
AMERICAN UNIVERSITY OF BEIRUT

ASSESSMENT OF THE PUNCHING SHEAR BEHAVIOR OF
INTERIOR SLAB-COLUMN CONNECTIONS
STRENGTHENED BY HEMP FIBERS SHEET FABRICS

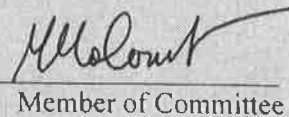
by
LOAI KHALED AL-MAWED

Approved by:

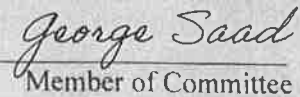
Dr. Bilal Hamad, Professor
Department of Civil and Environmental Engineering


Advisor

Dr. Mounir Mabsout, Professor
Department of Civil and Environmental Engineering


Member of Committee

Dr. George Saad, Associate Professor
Department of Civil and Environmental Engineering


Member of Committee

Date of thesis defense: April 28, 2021

ACKNOWLEDGEMENTS

I would like to express my deepest gratitude and appreciation to my advisor, Professor Bilal Hamad, for his continuous support and guidance throughout this research. I am very grateful to Professor George Saad for his comments and suggestions that contributed to clarifying certain aspects of this work and Professor Mounir Mabsout for reviewing this report and serving on the thesis committee.

Special thanks are extended to Mr. Helmi El-Khatib, Manager of Civil and Environmental Engineering Laboratories, and Ms. Dima Hassanieh, CEE Labs Assistant Manager, for their time, assistance, and helpful remarks.

I wish to express my appreciation to all the Civil and Engineering Laboratory staff. I would particularly like to thank Mr. Abdul Rahman Al-Sheikh and Mr. Bashir Asyala for their help throughout this project's experimental phase.

Many thanks to my engineering friends Mr. Mahmoud Khadija and Ms. Ruba Bashir, for supporting me throughout my graduate study.

ABSTRACT OF THE THESIS OF

Loai Khaled Al-Mawed

for

Master of Engineering

Major: Civil Engineering

Title: Assessment of the Punching Shear Behavior of Interior Slab-Column Connections Strengthened by Hemp Fibers Sheet Fabrics

The replacement of synthetic fibers by natural fibers such as hemp fibers in concrete has been investigated to achieve a sustainable construction material. Hemp fibers are extracted from the plant's stem, which makes them strong and stiff. These fibers are environmentally friendly and are used in the manufacturing of composite materials. In this research, the assessment of hemp fiber reinforced polymer (HFRP) fabric sheets' performance as punching shear strengthening material for interior slab-column connections is investigated experimentally. The experimental results were validated through numerical and analytical approaches. Twenty-four lab-scale interior slab-column connections (670x670 mm) were designed to experience punching shear failure. The main test variables are the slab thickness (55 or 75 mm), the ratio of steel reinforcement (1% or 1.5%), the width of hemp fiber fabric sheet (100, 150, or 200 mm), the number of layers of the HFRP sheets (one or two layers), the type of strengthening material (HFRP sheets or carbon fiber reinforced polymer (CFRP) sheets), and the location of hemp sheets (adjacent or offset by 1.5d from the face of the column). All tested specimens were loaded centrally through the column stub using the MTS universal testing machine up to failure. The assessment was based on a comparison of load capacity, mode of failure, load-displacement history, and cracking patterns of different specimens with different test parameters. Three finite element models were developed using ABAQUS software to predict the behavior of simulated specimens: un-strengthened specimen, specimen strengthened by HFRP, and specimen strengthened by CFRP. The experimental results demonstrate that HFRP strengthening sheets led to a significant improvement in the slab-column connections' structural behavior, depending on the slab thickness, steel content, width and configuration for HFRP sheets. The improvement in the ultimate shear capacity ranged between 5.5% and 41.14%, while the increase in stiffness reached up to 56.8% relative to the control specimen. It was found that although the natural confining HFRP sheet led to lower improvement in the performance of the strengthened specimen as compared to the synthetic CFRP sheet, the same improvement could be reached by the HFRP sheets when applied in larger width or in different configurations. The numerical findings show that the models predicted the connections' behavior in good agreement with the test results. The comparison between test results, available analytical model, and ACI Code shows that the analytical model provides good predictions for the test specimens' punching shear capacity. However, the ACI equations provide conservative predictions for the punching shear capacity of the test specimens.

TABLE OF CONTENTS

ACKNOWLEDGEMENTS	1
ABSTRACT	2
ILLUSTRATIONS.....	7
TABLES.....	11
INTRODUCTION.....	13
1.1. Introduction	13
1.2. Objectives and Scope	16
1.3. Thesis Outline.....	17
BACKGROUND AND LITERATURE REVIEW.....	18
2.1. Introduction.....	18
2.2. Hemp Fibers: Definition, Origin, Usage, Properties	18
2.2.1. Hemp Fiber Treatment	20
2.3. Applications of Different Natural Fibers as Strengthening Materials	21
2.4. Recent Research on Hemp Fibers Reinforced Polymer in Concrete Beams and Columns	24
2.5. Recent Research on Strengthening of Interior Slab-Column Connections Using Synthetic Fibers	26
EXPERIMENTAL PROGRAM	30
3.1. Introduction.....	30

3.2. Part One: Preliminary Trial Study	31
3.2.1. Materials	31
3.2.1.1. Concrete.....	31
3.2.1.2. HFRP Fabric Sheets.....	31
3.2.1.3. Adhesive	32
3.2.2. Test Specimens	33
3.2.3. Test Setup	34
3.2.4. Results and Discussion	35
3.2.4.1. Mode of Failure	35
3.2.4.2. Load-Displacement Behavior	37
3.2.5. Conclusions of the Preliminary Study	38
3.3. Part Two: Full-Scale Experimental Program	38
3.3.1. Test Variables	39
3.3.2. Materials	41
3.3.2.1. Concrete.....	41
3.3.2.2. Reinforcing Steel.....	41
3.3.2.3. HFRP Fabric Sheet	42
3.3.2.4. Carbon Fiber Reinforced Polymer (CFRP) Sheet	44
3.3.2.5. The Adhesive Sikadur-330	45
3.3.3. Fabrication of the Slab-Column Specimen	45
3.3.3.1. Formwork	45
3.3.3.2. Concrete Casting	46
3.3.3.3. Installation of the HFRP Fabric Sheets	46
3.3.4. Testing Program.....	48
3.3.4.1. Instrumentation	48
3.3.4.2. Test Setup	48
DISCUSSION OF TEST RESULTS AND ANALYSIS	50
4.1. Introduction.....	50
4.2. Mode of Failure	50
4.3. Test Results and Analysis	54

4.3.1. Series SA1	55
4.3.1.1. Influence of the Width of HFRP Sheets	55
4.3.1.2. Influence of Location of HFRP Sheets.....	58
4.3.1.3. Influence of the Type of Confining Sheet: HFRP versus CFRP	60
4.3.2. Series SA2.....	61
4.3.2.1. Influence of the Width of HFRP Sheets	62
4.3.2.2. Influence of Location of HFRP Sheets.....	63
4.3.2.3. Influence of the Type of Confining Sheet: HFRP versus CFRP	64
4.3.3. Series SB1	65
4.3.3.1. Influence of the Width of HFRP Sheets	66
4.3.3.2. Influence of Location of HFRP Sheets.....	67
4.3.3.3. Influence of Number of Layers of HFRP Sheets	68
4.3.3.4. Influence of the Type of Confining Sheet: HFRP versus CFRP	69
4.3.4. Series SB2	70
4.3.4.1. Influence of the Width of HFRP Sheets	72
4.3.4.2. Influence of Location of HFRP Sheets.....	72
4.3.4.3. Influence of Number of Layers of HFRP Sheets	73
4.3.4.4. Influence of the Type of Confining Sheet: HFRP versus CFRP	74
4.3.5. HFRP and CFRP Strains.....	75
NUMERICAL AND ANALYTICAL INVESTIGATIONS	77
5.1. Introduction.....	77
5.2. Part One: Numerical Modeling	77
5.2.1. Finite Element Method.....	77
5.2.2. Concrete Damaged Plasticity (CDP)	78
5.2.2.1. Literature	78
5.2.2.2. Concrete Damage Plasticity (CDP).....	79
5.2.3. Model 1: Compression Test for Concrete Cylinder (Material Verification) .	81
5.2.3.1. Laboratory Test	82
5.2.3.2. Finite Element Model	83
5.2.3.2.1. Model Geometry and Boundary Conditions	83
5.2.3.2.2. Calibration of the Model	84

5.2.4. Model 2: Slab-Column Connection	86
5.2.4.1. Finite Element Model	87
5.2.4.1.1. Model Construction	87
5.2.4.1.3. Materials	88
5.2.4.1.4. Calibration of the Model	89
5.2.4.2. Finite Element Results and Discussion	92
5.3. Part Two: Analytical Modeling	96
5.3.1. Analytical Model	96
5.3.2. American Concrete Institute (ACI) Building Code	99
5.3.3. Analytical Results and Discussion	100
CONCLUSIONS AND RECOMMENDATIONS	102
6.1. Conclusions	102
6.2. Recommendations	105
REFERENCES	106

ILLUSTRATIONS

Figure

1.1. Failure surface of punching shear	14
2.1. Hemp leaves.....	19
2.2. Reinforcement details for test specimens studied by Wang and Xian, (2020)	24
3.1. Test specimens used in the preliminary study to compare types of epoxies	33
3.2. Test specimens used in the preliminary study to check feasibility of the study ..	34
3.3. A schematic diagram of the test setup	35
3.4. Location of strain gauges	35
3.5. Typical crack pattern of specimens SA1-H10-Sikadur-300 and SA1-H10-Sikadur-330	36
3.6. Typical crack pattern of specimens SB1-Control and SB1-H15	36
3.7. Load-displacement responses of specimens SA1-H10-Sikadur-300 and SA1-H10-Sikadur-330	37
3.8. Load- displacement responses of specimens SB1-Control and SB1-H15	38
3.9. Slab-column connection 3D view	39
3.10. Test setup of the compression test of a concrete cylinder	41
3.11. Dimensions and reinforcement details of the slab specimen	42
3.12. Preparation of the HFRP fabric strips for tensile testing	43
3.13. Tensile test setup of the HFRP fabric strips	43
3.14. Mode of failure of the HFRP fabric strip.....	44
3.15. Stress-strain curve of the tested HFRP fabric strip.....	44
3.16. View of the formwork before concrete casting	45
3.17. Concrete batching	46
3.18. Levelling of the cast slab.....	46
3.19. Casting the column stub after placing a plywood piece above the cast slab.....	46

3.20.	View of the specimens placed in the curing room.....	46
3.21.	Mixing the two components of Sikadur-330.....	47
3.22.	Applying the epoxy layer before installing the HFRP sheet	47
3.23.	Saturation of the HFRP sheet with epoxy.....	47
3.24.	Installing the HFRP sheet above the epoxy layer	47
3.25.	Applying a rubber roller on the HFRP sheet.....	48
3.26.	View of the strengthened specimen	48
3.27.	Locations of the two strain gauges.....	49
3.28.	Test setup of the specimen	49
4.1.	Typical crack patterns at failure	51
4.2.	Failure of specimens confined and strengthened by HFRP sheets.....	52
4.3.	Failure of specimens confined and strengthened by CFRP sheets.....	53
4.4.	Load-deflection curves of specimens with different HFRP sheet width, Series SA1.....	56
4.5.	Load-deflection curves of specimens with different location of the HFRP sheet relative to the column face in Series SA1	59
4.6.	Load-deflection curves for specimens SA1-H15-A, SA1-H20-A, and SA1-F15-A.....	61
4.7.	Load-deflection curves of the control specimens SA1 and SA2, identical except for the reinforcement ratio.....	62
4.8.	Load-deflection curves of specimens with different HFRP sheet width, Series SA2.....	63
4.9.	Load-deflection curves of specimens with different location of the HFRP sheet relative to the column face in Series SA2	64
4.10.	Load-deflection curves of specimens SA2-H15-A, SA2-H15-O, and SA2-F15-A	65
4.11.	Load-deflection curves of the control specimens SA1 and SB1, identical except for the slab thickness and hence the slab to depth ratio	66
4.12.	Load-deflection curves of specimens with different HFRP sheet width, Series SB1	67
4.13.	Load-deflection curves of specimens with different location of the HFRP sheet relative to the column face in Series SB1	68

4.14.	Load-deflection curves for specimens SB1-H15-A and SB1-H15(2)-A	69
4.15.	Load-deflection curves for specimens SB1-H15-A, SB1-H15-O, and SB1-F15-A	70
4.16.	Load-deflection curves of the control specimens SB1 and SB2, identical except for the reinforcement ratio.....	71
4.17.	Load-deflection curves of specimens SA2 and SB2, identical except for the slab thickness and hence the slab to depth ratio	71
4.18.	Load-deflection curves of specimens with different HFRP sheet width, Series SB2.....	72
4.19.	Load-deflection curves of specimens with different location of the HFRP sheet relative to the column face in Series SB2	73
4.20.	Load-deflection curves for specimens SB2-H15-A and SB2-H15(2)-A	74
4.21.	Load-deflection curves for specimens SB2-H15-A, SB2-H15-A, and SB2-F15-A	74
4.22.	Typical load versus strain response for (a) CFRP sheets and (b) HFRP sheets..	75
5.1.	The yield surface in: (a) plane stress cross section and (b) deviatory plane; Lubliner et al. (1989).	80
5.2.	Response of concrete to uniaxial loading in (a) tension and (b) compression; ABAQUS (2010)	81
5.3.	The concrete sample subjected to compression test	82
5.4.	Stress-strain relationship for the concrete	82
5.5.	3D representation of the model.....	83
5.6.	Boundary conditions used in the numerical model.....	83
5.7.	Experimental vs. Numerical results for different mesh sizes	84
5.8.	Stress-strain curves using different values of viscosity parameter	86
5.9.	Geometry and boundary conditions of Model 2	88
5.10.	Experimental vs. Numerical results for different mesh sizes	90
5.11.	Mesh scheme and springs representation.....	91
5.12.	Load-displacement response for the numerical model with different values of (K)	91
5.13.	Deflection shape at failure load	92

5.14. Comparison of crack patterns (a) SB1; (b) SB1-H15-A; and (c) SB1-F15-A	93
5.15. Load-deflection responses (a) SB1; (b) SB1-H15-A; and (c) SB1-F15-A	95
5.16. Strain, stress, and force distribution in section.....	97

TABLES

Table

2.1. Properties of hemp fibers as determined by several studies	20
3.1. Materials quantities used in the concrete mix	31
3.2. Dimensions of the used Hemp fabrics sheets.....	32
3.3. Mechanical properties of the epoxy Sikadur-330 and Sika dur-300.....	32
3.4. Test variables	40
3.5. Mechanical characteristics of the steel bars	42
3.6. The properties of the CFRP SikaWrap-230 C.....	44
4.1. Summary of the test results	57
4.2. Measured (HFRP-CFRP) ultimate strain.....	76
5.1. Concrete parameters	81
5.2. Concrete properties	82
5.3. Mesh sizes and No. of elements for the concrete cylinder	85
5.4. Material properties of adhesive.....	87
5.5. Damage properties of concrete	89
5.6. Steel reinforcement properties for Model 2	89
5.7. Composite material properties for Model 2	89
5.8. Comparison between experimental and numerical results	94
5.9. Comparison between experimental and analytical results.....	101

To My Beloved Family

CHAPTER 1

INTRODUCTION

1.1. Introduction

Evaluation indicators of civil engineering projects include serviceability, strength, durability, and cost. In most cases, the main concerns in building structures are having good performance and minimizing cost, while minor considerations are given to sustainability and environmental impact. Many buildings nowadays are constructed using a flat concrete slab system. Flat plate structural systems are composed of flat slabs supported directly on columns without beams. The advantages of using a flat plate system include faster construction, reducing floor-to-floor height, and more economical construction compared to other structural systems. However, in the flat slab, the connection between column and slab is typically the most critical part of its susceptibility to punching shear failure.

Punching shear failure is a brittle and non-ductile failure that has caused the collapse of many flat plate structures in the last century (King and Delatte 2004; Mirzaei.Y and Sasani.M 2011). When slab-column connections of the flat plates are subjected to heavy vertical loading, cracks will occur inside the slab around the column. These cracks extend across the slab's thickness at an angle of 20-45 degrees to the bottom side of the slab (**Figure 1.1**). Eventually, a punching shear failure of the slab will occur, which could lead to a progressive collapse of the entire structure.

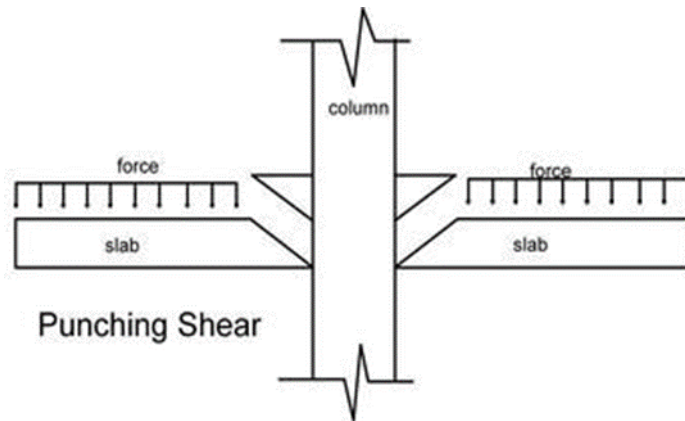


Figure 1.1 Failure surface of punching shear

Punching shear strength of flat slabs can be inadequate due to changing the building's use, increasing the floor loading, installing a new slab opening in the column's vicinity, corrosion of the reinforcement, and design construction errors. In these situations, the slab must be replaced or strengthened.

Strengthening could be more cost-effective than the replacement of the slab. Several techniques have been adopted to strengthen slab-column connections in flat plate structures. These techniques include transverse reinforcement pre-stressed against the slab surface, structural steel beams attached to the face of the column and bottom surface of the slab that act as column capitals, providing drop panel around the column, or by installing a combination of steel plates and transverse pre-stressed steel bolts on the top and bottom surfaces of the slab.

In the past two decades, several studies have investigated the effectiveness of using Carbon Fiber-Reinforced Polymer (CFRP) sheets as a strengthening technique for slab-column connections (Harajli and Soudki 2003; Soudki, El-Sayed, and Vanzwol 2012). These studies have shown that the feasibility and efficiency of using CFRP to enhance the connection's punching shear strength. The advantages of using CFRP sheets include: CFRP sheet is a lightweight and non-corrosive material, it is easy and quick to

apply, it does not require expensive equipment and skillful labor, and it does not change the appearance of the structure. The behavior of CFRP in shear strengthening of slab-column connections has been extensively studied and is well-understood.

On the other hand, with the rise of environmental issues, using natural products such as bio-based fibers are becoming more popular than synthetic polymers. Some natural fibers have desirable physical and mechanical properties, such as hemp, banana, coir, jute, flax, sisal, etc., which can replace synthetic fibers.

Strengthening concrete elements using natural fibers instead of synthetic fibers has many environmental benefits.

- First, natural fibers are renewable materials found anywhere in the world without consuming non-renewable fossil resources in their production.
- Second, natural fibers are Carbon neutrality; they have zero carbon footprints. The difference between carbon dioxide absorbed by natural fibers during their growth and carbon dioxide released in the atmosphere during the production, use, and disposal of these fibers is zero.
- Third, the accumulation of non-degradable polyethylene (PE) in the soil leads to serious environmental problems; however, using biodegradable natural fibers can reduce these problems.

As a result, the replacement of synthetic fibers by natural fibers will cause less harmful environmental impacts, which will lead to sustainable development (Sen and Jagannatha Reddy 2013).

1.2. Objectives and Scope

Recently, the replacement of synthetic fibers with natural fibers in concrete has been investigated to counter the growing environmental and sustainable issues. The purpose of this study is to examine the viability of using hemp fiber-reinforced polymer (HFRP) fabric sheets for punching shear strengthening of reinforced concrete two-way slabs. The research's novelty stems from the fact that no study is published in the literature on using hemp fiber fabrics to strengthen the interior slab-column connection. The work program is designed to assess experimentally, and numerically the load capacity and load-displacement response of small-scale reinforced concrete interior slab-column connections strengthened by HFRP fabric sheets. To achieve these objectives, twenty-four small-scale interior reinforced concrete 670x670 mm slab-column connection specimens, each with a 100x100 mm center column stub extending 150 mm from the slab's top surface and 50 mm from the bottom surface, were tested by using the Universal Testing Machine (MTS). The main test variables in this study include the slab thickness (55 or 75 mm), the ratio of steel reinforcement (1% or 1.5%), strengthening material (HFRP fabric sheets or carbon fiber reinforced polymer (CFRP) sheets), the width of HFRP fabric sheets, the number of HFRP layers, and the location of HFRP strips (adjacent or offset by $1.5d$ from the face of the column where d is the effective depth of the slab). Evaluation of the hemp fiber sheets' effectiveness was determined by comparing the structural behavior of different specimens fabricated with varying test parameters. Comparison was based on load capacity, mode of failure, load-displacement history, and cracking patterns. A numerical model was developed using the finite element software package (ABAQUS) to predict the maximum punching

shear load and deformation capacity. The experimental and numerical findings were evaluated to determine whether the numerical model provides accurate predictions.

1.3. Thesis Outline

This thesis is arranged into six main chapters. Chapter 1 presents an introduction to flat plates and the advantages of using natural fibers as an alternative to synthetic fibers and summarizing the research objectives and program. Chapter 2 provides an overview of natural fibers such as hemp fibers as a strengthening material for reinforced concrete elements and summarizes previous investigations related to strengthening interior slab-column connections using synthetic fibers. The experimental program is discussed in Chapter 3, including the test specimen, the test setup, and materials used. Chapter 4 presents and analyzes the experimental test results regarding load-deflection response, mode of failure, and cracking patterns for each specimen. Chapter 5 explains the numerical procedures, also presents a comparison between the numerical and experimental results. The analytical investigation is also presented in Chapter 5. Chapter 6 summarizes the conclusions of this study and the recommendations for future research work.

CHAPTER 2

BACKGROUND AND LITERATURE REVIEW

2.1. Introduction

The first part of this chapter presents an overview of natural fibers, particularly hemp fibers, and information from existing research studies on using natural fibers as strengthening material for different reinforced concrete components. The second part introduces recent research from the literature on the feasibility of enhancing interior slab-column connections using synthetic fibers (externally bonded CFRP or GFRP sheets). The behavior of the strengthened slab-column connections has been investigated thoroughly and is well understood. On the other hand, it is worth mentioning that some reported studies have shown improvement in the behavior of various structural elements strengthened by natural fibers. However, little information exists on externally applied hemp fiber fabric sheets on interior slab-column connections.

2.2. Hemp Fibers: Definition, Origin, Usage, Properties

Hemp is naturally one of the most environmentally friendly fibers and also the oldest. Hemp fibers are extracted from the Cannabis Sativa L plant stem and belong to the family of cannabis. Hemp is an annual crop grown over 12,000 years ago. This plant is now mainly found in Central Asia, European Union, China, and the Philippines (Shahzad 2012). The view of the hemp plant is shown in **Figure 2.1**.

In the hemp plant, fibers are found in the stems' tissues, which provide the plant's strength and stiffness. The essential components of hemp fibers are cellulose,

hemicellulose, lignin, and pectin. These components describe the physical properties of the fibers. The stiffest and strongest organic constituent in the fibers is cellulose (Shahzad 2012).



Figure 2.1 Hemp leaves

Hemp fibers are primarily used in a range of commercial products, including ropes, textiles, clothing, shoes, and food. Nowadays, due to the potential of hemp fibers' physical properties, they are used in the construction industry as insulation materials, building materials, paper, and pulp (Keller 2013).

The primary deficiency of hemp fiber is the uncertainty of its physical and mechanical properties due to its composition variability. Many factors may influence the variability in diameters and properties of natural fibers. Some of these factors include source, age, geographic origin and rainfall during growth, etc. (Rahman Khan et al. 2011).

Several factors that affect the variability in the physical and mechanical properties of natural fibers have been identified by (Nishino 2004). According to the author, these factors are divided into materials and measurement conditions. Materials conditions include (i) Microscopic: crystallinity, microfibril angle, and crystal

modifications, (ii) Macroscopic: fineness, porosity, size, and shape of the lumen; and (iii) History, source, age, retting and separating conditions, geographical origin, and rainfall during growth. Measurement conditions include tensile test speed, initial gauge length, moisture, temperature, and cross-section of fibers at different points.

Several studies have been carried out to investigate the mechanical properties of hemp fibers. **Table 2.1** reports some of hemp's mechanical properties from the literature.

Table 2.1 Properties of hemp fibers as determined by several studies

Source	Average diameter (μm)	Young's modulus (GPa)	Tensile strength at break (MPa)	Elongation at break (%)	Tensile deformation speed (mm/min)
Eichhorn and Young, (2004)	31.2 \pm 4.9	19.1 \pm 4.3	270 \pm 40	0.8 \pm 0.1	1
Bourmaud and Baley, (2009)	17.7	44.5	778	1.8	1
Placet, (2009)	42	14.4	285	2.2	0.6
Fan, (2010)	37.42 \pm 6.62	-	529 \pm 12.35	-	1
Duval et al., (2011)	17.1 \pm 4.5	19.6 \pm 14.8	482 \pm 337	3.0 \pm 1.5	1
Placet et al., (2012)	27.6 \pm 7.5	24.7 \pm 11.4	646 \pm 253	2.1 \pm 0.7	0.12

2.2.1. Hemp Fiber Treatment

Two treatment techniques have been adopted to enhance the hemp fiber-concrete matrix interface: physical and chemical treatment.

- Physical treatment does not modify the fibers' chemical components, but it improves the mechanical bonding to polymers. The most used physical treatment techniques are stretching, thermo-treatment, clattering, cold plasma treatment, etc.
- Chemical changes occur when the reactive components of the natural fibers react with chemical agents resulting in a covalent bond between both. Chemical treatment is about adding coupling agents to the natural fibers. As it is known that natural fibers contain incompatible hydroxyl groups (OH), the coupling

agents react with the hydroxyl group of cellulose to bring out the compatibility of the elements that lead to some changing of surface tension, impregnation of fibers, and chemical coupling (George, Sreekala, and Thomas 2001). Such changes significantly improve the characteristic performance of composites. The most widely used chemical treatments for natural fibers are liquid ammonia, esterification, silane coupling method, etc.

2.3. Applications of Different Natural Fibers as Strengthening Materials

Sen and Jagannatha Reddy, (2013) compared the effectiveness of using natural jute fiber fabric composite (JFRP) to improve the flexural strength of RC beam with artificial Carbon fiber reinforced polymer (CFRP) and glass fiber reinforced polymer (GFRP). The researcher studied a total of fourteen beams designed to fail in pure flexure. The experimental program contained three groups. Group A consisted of two duplicate control specimens; Group B consisted of six beams (3 with three replicates) strengthened by full-length U-wrapping using a single layer of jute, Carbon, or Glass FRP. Group C included six beams (3 with three replicates) designed to investigate the effect of U strips wrapping using a single layer of jute, CFRP, or GFEP on the flexural strength of the beam. All beams have the same reinforcement detailing with a reinforcement ratio of 0.89%. The tested specimens were subjected to three-point loading until failure. They concluded that natural jute FRP, like artificial CFRP and GFRP, can improve RC beams' ultimate flexural strength. These improvements reach 62.5%, 150%, and 125% for the beams strengthened by JFRP, CFRP, and CFRP, respectively, with full-length wrapping scheme, and by 25%, 50%, and 37.5%,

respectively, with strip wrapping scheme. It is worth mentioning that JFRP strengthening displayed the highest deformability index.

Sen and Reddy, (2014) also investigated the effect of using natural sisal fabric reinforced polymer (SFRP) on RC beams' flexural strength. A comparative study was done between SFRP and the other two artificial fibers, carbon fiber reinforced polymer (CFRP) and glass fiber reinforced polymer (GFRP), to determine the feasibility of using SFRP as an alternative to synthetic fibers. The authors adopted the same previous work program (14 RC beams in three groups A, B, and C) and the same test variables (wrapping techniques: full wrapping and strip wrapping techniques). The researchers concluded from experimentations of RC beams subjected to bending that SFRP is similar to artificial CFRP and GFRP in terms of its ability to increase flexural strength and improve RC's load-deflection behavior beam. Compared with the un-strengthened control beams, beams with full sisal FRP wrapping recorded 112.5% increases in ultimate flexural capacity and improved ductile failure, and beams with only strip sisal wrapping recorded 65.2% increases in ultimate flexural capacity.

Sen and Paul, (2015) conducted an experimental investigation on a total of 18 cylindrical concrete specimens confined by four different types of fiber composites (two natural fiber composites: sisal and jute FRP, and two artificial fiber composites carbon and glass FRP) to understand the effect of these composites on the confinement strength of concrete cylinders. The study's test parameters were the strengthening materials (SFRP, JFRP, CFRP, and GFRP) and the confinement configuration (full wrapping and 50% wrapping configuration). All concrete cylinders with 103 mm diameter and 200 mm height were subjected to monotonic axial compressive loads until failure. Sen and Paul (2015) concluded that natural fibers (SFRP and JFRP) also have the potential to

enhance the axial load capacity of concrete cylinders similar to artificial fibers (CFRP and GFRP). Although the natural fibers exhibited lower improvement in concrete cylinders' load capacity than synthetic fibers, this improvement was superior combined with these fibers' environmental and sustainable benefits.

Wang and Xian, (2020) performed an experimental study for improving the shear capacity of reinforced concrete beams. The RC beam specimens were strengthened by ordinary flax fiber sheets and flax fiber sheets grafted with nano-TiO₂. Five RC beams with a length of 1800 mm and a cross-section of 200x400 mm were tested (**Figure 2.2**). Besides the control beam, two beams were strengthened by three and six layers of ordinary flax fiber sheets, one beam was strengthened with three layers of flax fiber sheets grafted with nano-TiO₂, and the fifth beam was strengthened by synthetic basalt fiber. Only in the left half-span of the beam specimens, a certain number of stirrups are provided to ensure that the shear failure occurs only in the right-half span. However, the right-half span is strengthened by U-shaped reinforcement fiber sheets with 300 mm width and 1000 mm length. All specimens were tested under a three-point bending load until failure. The experimental results demonstrated that providing reinforcing flax fabric sheets on the beam significantly increases its shear capacity and mid-span deflection up to 72.8% and 75.9%, respectively, compared to the unreinforced RC beams.

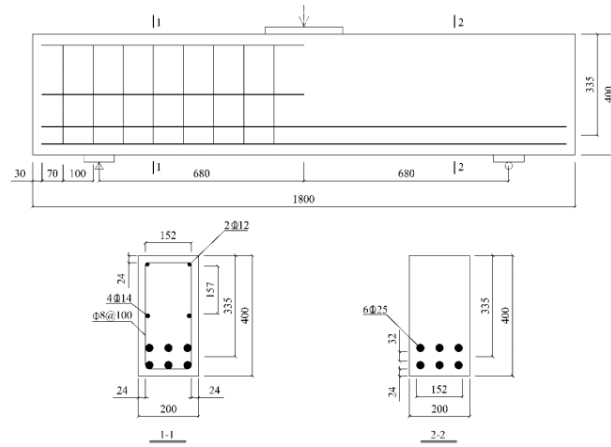


Figure 2.2 Reinforcement details for test specimens studied by Wang and Xian, (2020)

2.4. Recent Research on Hemp Fibers Reinforced Polymer in Concrete Beams and Columns

Yinh et al., (2016) tested five full-scale reinforced concrete beams to investigate the efficiency of sheets of epoxy bonded HFRP composites in the flexural strengthening of RC beams. All beams were designed for flexural failure. Four-point load bending was applied to the specimens until failure. Variables included fiber sheet thickness (one or two layers) and strengthening configuration (tension side only or U-wrap). Test results showed that HFRP sheets could significantly increase the flexural strength and stiffness of original RC beams. Increasing the thickness of the HFRP sheets led to an increase in flexural strength. The performance of strengthened beams in the U-wrapped scheme was more efficient to strengthen the beam than the tension side scheme.

Ghalieh et al., (2017) reported an experimental study to test the effectiveness of HFRP sheets as external confinement for concrete columns. Axial compression test was done on 30 concrete cylinders using an MTS machine with a constant 3 mm/min displacement rate. The main test variables included the number of confining layers (the number of confinement layers ranged between one, two, and four) and the column slenderness ratio (the different slenderness ratios checked were 1.5, 2, 2.5, and 3). Test

results indicated that the HFRP sheets improved the reinforced concrete column's axial compressive strength and ductility. This improvement increased as the thickness of the hemp fiber sheet increased. They concluded that the ultimate strength and the ductility enhancement of the HFRP confined RC columns decreased with the increase of slenderness ratio.

Siriluk et al., (2018) conducted an experimental study to examine the effectiveness of HFRP sheets in enhancing the shear strength of reinforced concrete deep beams. HFRP sheets were bonded to the exterior surface of the beams using epoxy resin. All beams were tested under three-point loading; the load was applied in the middle of the beam. The test parameters included the thickness of the HFRP sheet and the strengthening configuration (both-side bonded or three-side bonded U shape). Experimental results revealed that HFRP sheets improved the shear ultimate load and deflection capacity of the RC deep beams. The thickness of the sheets had a significant impact on shear strengthening, whereby the shear strength of the RC deep beam increased upon increasing the sheet thickness. They also found that the U-shape strengthening configuration was more effective than both sides bonded.

Recent research was conducted at the American University of Beirut using hemp fiber-reinforced polymer sheets for improving the out-of-plane flexural capacity of unreinforced masonry walls (Bitar et al. 2020). The main test parameters included reinforcement ratio (0.381%, 1.2% or 2%), the configuration of HFRP sheets (hemp fiber strips or fully wrapped wall), number of the HFRP layers (one or two layers), and inclusion of anchors (additional fabric covered on the wall back in the U shape). Five small-scale masonry walls were built of normal weight hollow concrete masonry blocks. Then hemp fiber composite sheets were bonded to the exterior surface of the

walls using epoxy resin. The specimens were then subjected to four-point monotonic load bending until failure. The effectiveness of HFRP sheets was evaluated by analyzing the flexural capacity, ductility, and failure modes of the wall specimens. Test results indicated that strengthening the unreinforced masonry wall by HFRP sheets significantly improved its out-of-plane flexural capacity. This improvement increased upon increasing the sheet layers. The experimental findings showed the importance of anchors in increasing wall ductility. The common mode of failure of strengthened walls was a rupture of the sheets, while the mode was a shear failure for the walls with a reinforcement ratio of 2% where the hemp composites did not reach their ultimate tensile strength.

2.5. Recent Research on Strengthening of Interior Slab-Column Connections Using Synthetic Fibers

Harajli and Soudki, (2003) conducted an experimental study to investigate the enhancement in shear strength of interior slab column connection by using externally bonded flexible Carbon Fiber Reinforced Polymer (CFRP) sheets. The test program included sixteen small-scale interior connections, each consisting of a 670x670 mm square slab with a 100x100 mm center column stub. The specimens were built using a concrete mix with a target cylinder compressive strength of 34.5 MPa (5,000 psi). The test parameters included the thickness of the slab (55 or 75 mm), the ratio of steel reinforcement (1% or 1.5%), and the area of CFRP sheets. The specimens were split into four groups based on the slab thickness and the amount of steel reinforcement. Group 1 had four specimens with slab thickness 55 mm and steel reinforcement ratio of 1% and various CFRP widths. Group 2 had the same slab thickness as group 1 but with a reinforcement ratio of 1.5%. The reinforcement ratio in groups 3 and 4 was similar to

that in groups 1 and 2, respectively, but the slab thickness was 75 mm. All specimens were supported over the four edges and then subjected to point load through the column stub until failure using MTS universal testing machine. Test results showed that externally bonded CFRP sheets considerably enhanced the flexural strength and the shear capacity of the interior slab-column connection. This enhancement varied based on the slab thickness, amount of steel reinforcement, and area of CFRP sheets. Furthermore, they concluded that the increase in flexural strength due to the use of CFRP might change the failure mode of the connection from pure flexural to a combined flexural-shear mode or pure punching mode; however, it reduced failure ductility.

Chen et al., (2006) investigated Glass Fiber-Reinforced Polymer Laminates' use as strengthening material for interior concrete slab-column connections to improve its punching shear capacity. They tested eighteen specimens, each consisting of a 1000x1000x100 mm square slab with a 150x150 mm square column extending 150 mm from the top of the slab surface. The test parameters included concrete compressive strength (14 or 28 MPa), tension steel reinforcement ratio (0.59% or 1.31%), and the number of GFRP laminate layers (one or two layers). Test results indicated that GFRP laminates markedly enhanced the ultimate punching shear capacity for interior slab-column connections. This enhancement was influenced by the concrete compressive strength, steel reinforcement ratio, and the number of layers of GFRP laminates. The enhancement of GFRP laminates was more effective for slabs with low compressive strength and reinforcement ratio. It was concluded that using GFRP laminates could change the mode of failure of the connection from flexural failure to punching shear failure.

Harajli et al., (2006) evaluated a new strengthening technique to enhance slab-column connections' punching shear capacity. The technique involved drilling shear bolts into holes and pre-stressing them against the concrete surface combined with externally bonded FRP sheets on the slab's tension face. Small-scale interior slab-column connections were tested. The intended concrete compressive strength was 30 MPa for all tested specimens. The main test variables included slab span-depth ratio, steel reinforcement ratio, CFRP area, and the area and configuration of steel bolts. They found that using steel bolts only increased the punching shear capacity, leading to improve the connection's ductility. However, using a combination of steel bolts with bonded CFRP sheets increased the flexural strength and the shear capacity of the slab.

Erdogan et al., (2007) evaluated a new CFRP strengthening method for enhancing the punching shear strength of reinforced concrete interior slab-column connections. The method consisted of using self-manufactured CFRP dowels installed in pre-drilled holes around the column stubs of the specimens, and then the end of the dowels was fanned out and bonded on the CFRP strips. Four full-scale slab-column specimens consisting of a 2300x2300x150 mm slab and a 250x250x300 mm column extending from both slab faces were tested. All specimens were cast using concrete compression strength f'_c of 30 MPa and tension longitudinal reinforcement ratio of 1.41%. The test parameter was the number of CFRP dowels around the column stub. Three of four test specimens were strengthened by this technique, while one was the un-strengthened control specimen. The test results clearly showed that the new method of using CFRP dowels considerably enhanced the ultimate punching shear load capacity, ultimate displacement, and the strengthened connections' residual capacity.

Chen and Chen, (2020) investigated the effectiveness of using carbon fiber-reinforced polymer (CFRP) laminates, externally bonded on the tension side of concrete slab-column connections, on the punching shear capacity. They tested twelve specimens. The slab was 1000x1000x100 mm, and the column was 150x150 mm. The test variables included the concrete compression strength f'_c (14 or 28 MPa), the tensile steel reinforcement ratio (0.6% or 1.2%), and the number of layers of CFRP laminates (one or two layers). The concrete slab was simply supported along the four edges. They were then subjected to a concentrated load through the column's stub and were loaded until failure. Each slab was analyzed based on its punching shear strength, stiffness, and mode of failure. Test results indicated that externally bonded CFRP laminates significantly improved the tested slab-column connections' punching shear strength. Slabs with a lower reinforcement ratio strengthened by CFRP laminates exhibited a distinct enhancement in connection's shear strength.

CHAPTER 3

EXPERIMENTAL PROGRAM

3.1. Introduction

Prior to launching this study's experimental program, a preliminary trial study was conducted on four small-scale reinforced concrete interior slab-column connections. The first objective of this study was to check the feasibility of using HFRP fabric sheets to strengthen interior slab-column connections before starting the large-scale study. The second objective was to check the feasibility of using epoxy sikadur-330 to bond the HFRP fabric strips on the slab's tension side instead of epoxy sikadur-300, which was used in reported research on hemp fabrics. The need to use the sikadur-330 type is to compare the behavior of specimens strengthened by HFRP fabric sheets with those strengthened by CFRP strips where the manufactured company of CFRP sheets recommends the sikadur-330 type. All four specimens were loaded centrally through the column stub with monotonically increased load until failure using the MTS Universal Testing machine.

The preliminary trial study's promising results made possible the design of the second part of the experimental program. Twenty-four reinforced concrete interior slab-column connections were prepared with different test parameters that could affect the behavior and effectiveness of using HFRP fabrics as strengthening material for interior slab-column connections. The main test parameters are the slab thickness (55 or 75 mm), the ratio of steel reinforcement (1% or 1.5%), type of strengthening material (HFRP or CFRP sheets), the width of the HFRP fabric sheets, the number of sheets layers, and the location of the HFRP strips (adjacent to the column or offset by 1.5d

from the face of the column). The specimen details are presented, the materials used are described and tested, and the load setup is explained.

3.2. Part One: Preliminary Trial Study

3.2.1. Materials

3.2.1.1. Concrete

Normal strength concrete mixes were prepared using a small mixer in the Materials laboratory of the American University of Beirut to achieve a compressive strength of 35 MPa. The quantities of each material in the mix per cubic meter of concrete are listed in **Table 3.1**.

Table 3.1 Materials quantities used in the concrete mix

	Cement	Coarse Aggregate	Fine Aggregate	Water
Description	Portland Cement Type I	Well-graded crushed limestone aggregates with a maximum size of 10 mm	Sand	-
Weight (kg)	485	1265	630	242.5
Ratio	1	2.6	1.3	0.5

Each batch was used to cast one specimen and three 150x300 mm standard cylinders. The specimen and the cylinders were cured for 28 days. The compressive strength was determined at seven days, 28 days, and on the testing day.

3.2.1.2. HFRP Fabric Sheets

Commercial bidirectional HFRP fabric sheets were used. The fabrics were cut into designated sizes to strengthen the interior concrete slab-column connections in the

preliminary study. The number of fabric strips, the sheet length, and the sheet width used for each specimen are presented in **Table 3.2**.

Table 3.2 Dimensions of the used Hemp fabrics sheets

Specimens	Number of strips used	Length (mm)	Width (mm)
SA1-H10-A-SIKADUR300	4	670	100
SA1-H10-A-SIKADUR330	4	670	100
SB1-Control	0	-	-
SB1-H15-A	4	670	150

3.2.1.3. Adhesive

Two types of adhesives were used in the preliminary study, namely (Sikadur-300 and Sikadur-330). The feasibility of using Sikadur-300 to bond hemp fabric sheets to concrete was proved in different researches (Ghalieh et al. 2017; Bitar et al. 2020). In order to compare the behavior of specimens strengthened by natural HFRP fabrics with specimens strengthened by synthetic CFRP strips, it was preferred to use the same type of bonding adhesive. The manufacturing company recommends Sikadur-330 to bond CFRP to concrete. Therefore, a comparative study was done on two specimens, one strengthened by 670x100 mm hemp fabric strips bonded to the tension side of the connection using sikadur-300 and the other identical to the first except for the use of sikadur-330. The mechanical properties of the two types of epoxies provided by the supplier are given in **Table 3.3**.

Table 3.3 Mechanical properties of the epoxy Sikadur-330 and Sikadur-300

Property	Sikadur-330	Sikadur-300
Tensile Strength (MPa)	30 (7 days at +23°C)	45 (7 days at +23°C)
Tensile Modulus (MPa)	4,500 (7 days at +23°C)	3,500 (7 days at +23°C)
Elongation at Break (%)	0.9 (7 days at +23°C)	1.5 (7 days at +23°C)
Flexural Modulus (MPa)	3,800 (7 days at +23°C)	2,800 (7 days at +23°C)

3.2.2. Test Specimens

The first two reinforced concrete interior slab-column connections were constructed with the same geometrical configuration and steel reinforcement details. The slab dimensions were 670x670 mm and 55 mm thick, each with a 100x100 mm center column stub extending 150 mm from the slab's top surface and 50 mm from the bottom surface. Each slab was reinforced by one bottom layer of 8 mm steel bars, spaced at 162.5 mm c/c in each direction, with the average effective depth to the center of the two reinforcing bar layers of 37 mm. Four vertical 8-mm deformed steel bars were placed at the corners of the column stub. The specimens are shown in **Figure 3.1**. The specimen in **Figure 3.1a** was strengthened by 670x100 mm HFRP fabric strips bonded to the concrete connection's tension side using epoxy sikadur-300 and is designated as SA1-H10-Sikadur-300. The specimen in **Figure 3.1b** is identical to the first one except for using sikadur-330 and is designated as SA1-H10-Sikadur-330.

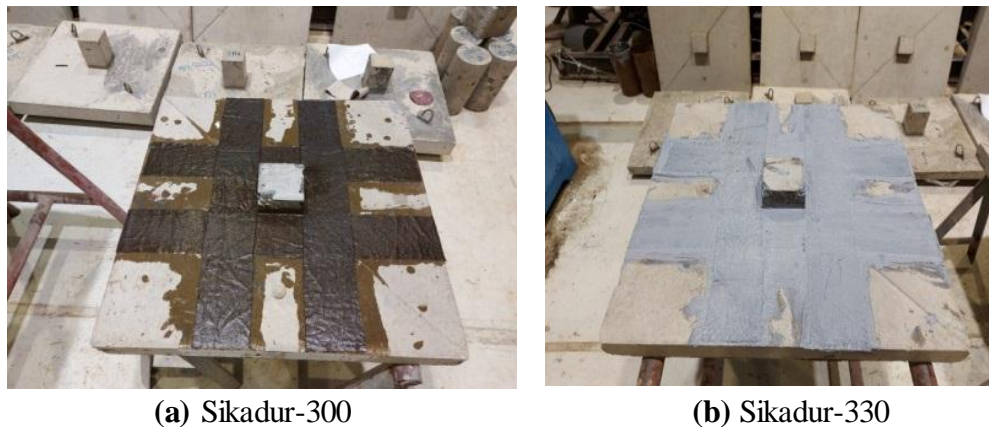


Figure 3.1 Test specimens used in the preliminary study to compare types of epoxies

Two other specimens were built to check the effectiveness of HFRP fabric sheets on the interior slab column connection's punching shear capacity. Both specimens had the same concrete compressive strength, geometrical configuration, and reinforcement details. Each specimen with dimensions 670x670 mm and 75 mm thick

was reinforced by one bottom layer of 10 mm steel bars, spaced at 162.5 mm c/c in each direction with an average effective depth to the center of two layers of 55 mm. With reference to **Figure 3.2**, the first specimen was the control specimen with no HFRP sheet strengthening and is designated as SB1-Control, and four HFRP fabric strips with dimensions strengthened the second one 670 x150 mm and is designated as SB1-H15.

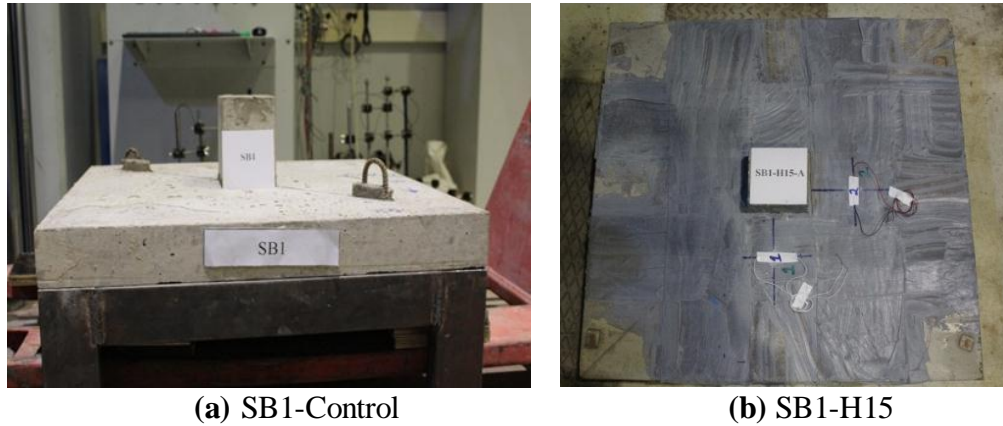


Figure 3.2 Test specimens used in the preliminary study to check feasibility of the study

3.2.3. Test Setup

All specimens were mounted on a steel frame with 40 mm wide pedestals on all four sides and were loaded centrally through the column stub with monotonically increased load until failure using the MTS Universal Testing machine. Average deflections at the center of the slab were measured using two linear variable differential transducers (LVDT) placed in opposite directions attached to the horizontal plate extending from the column stub's top. A schematic diagram of the test setup is shown in **Figure 3.3**. The strains in the HFRP strips were measured using strain gauges attached at the mid-width at the slab's maximum negative moment (at the junction of the slab and the column), as shown in **Figure 3.4**.

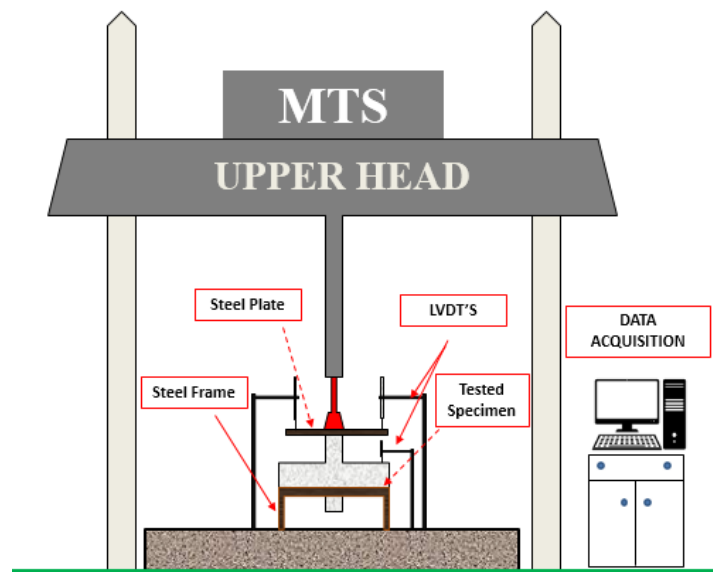


Figure 3.3 A schematic diagram of the test setup

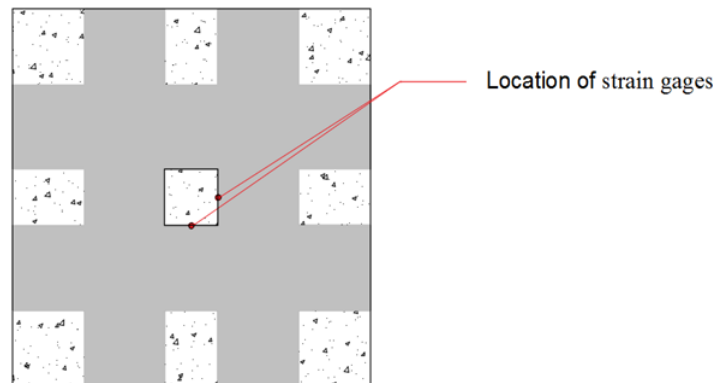


Figure 3.4 Location of strain gauges

3.2.4. Results and Discussion

3.2.4.1. Mode of Failure

Figure 3.5 shows the failure patterns of the SA1-H10-Sikadur-300 and SA1-H10-Sikadur-330 specimens. Both specimens exhibited the same flexural failure mode where diagonal cracks propagated from the column stub towards the corner of the slab. The failure of the two specimens was preceded by breaking the HFRP fabric sheets in the critical maximum moment region (at the mid-length of the hemp layers). De-bonding of the hemp sheets was observed in both specimens along the major crack of the specimen.

Figure 3.6 shows the typical crack pattern at the failure load of specimens SB1-control and SB1-H15. Both specimens experienced punching shear failure where a sudden punching of the column stub through the slab at the compression face occurred. The punching shear failure plane was clearly observed on the tension side of specimens SB1-control; the distance from the face of the column stub to the punching shear plane ranged from 170 to 230 mm. Breaking of two HFRP fabric sheets at their mid-length can be seen in specimen SB1-H15. Also, delamination of the sheets occurred along the major cracks in specimen SB1-H15.

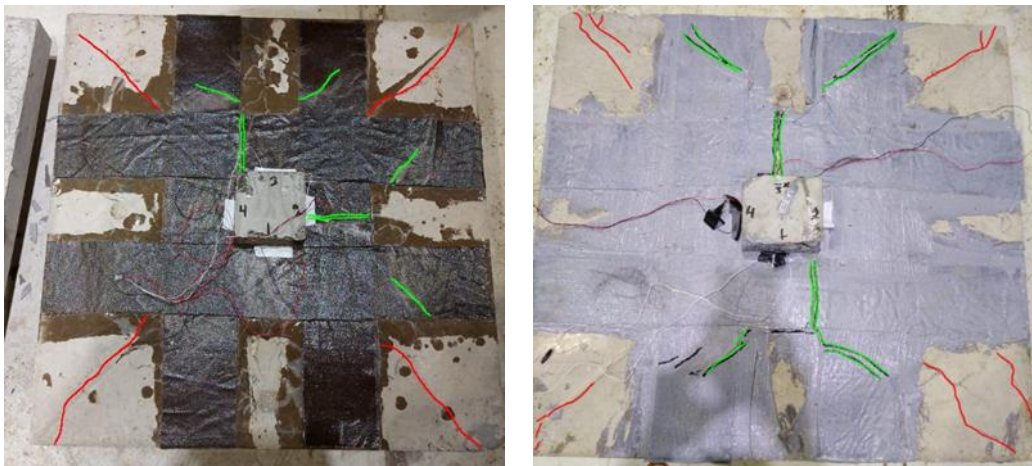


Figure 3.5 Typical crack pattern of specimens SA1-H10-Sikadur-300 and SA1-H10-Sikadur-330



Figure 3.6 Typical crack pattern of specimens SB1-Control and SB1-H15

3.2.4.2. Load-Displacement Behavior

The load-displacement responses for specimens SA1-H10-Sikadur-300 and SA1-H10-Sikadur-330 are plotted in **Figure 3.7**. In general, both curves display an approximate same bi-linear behavior and can be divided into a stiff pre-cracking stage of the RC specimen followed by a linear elastic stage until failure occurred. It can be seen by comparing the load-displacement responses that both specimens reached almost the same ultimate load ≈ 51.5 kN.

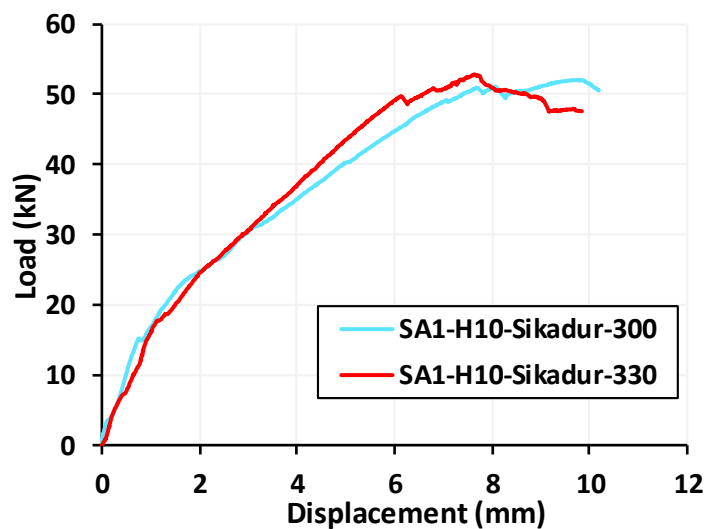


Figure 3.7 Load-displacement responses of specimens SA1-H10-Sikadur-300 and SA1-H10-Sikadur-330

Figure 3.8 compares the load-displacement curves for specimens SB1-Control and SB1-H15. Both curves display a sharp drop in the load immediately after the ultimate load is reached. The specimen strengthened by HFRP fabric sheets SB1-H15 exhibited a stiffer response in the pre-ultimate stage compared to the un-strengthened specimen SB1-Control. The control specimen's ultimate load was 94 kN, and that of SB1-H15 was approximately 100.9 kN. Strengthening the HFRP fabric sheet enhanced the ultimate punching shear capacity of the slab by approximately 7.34%.

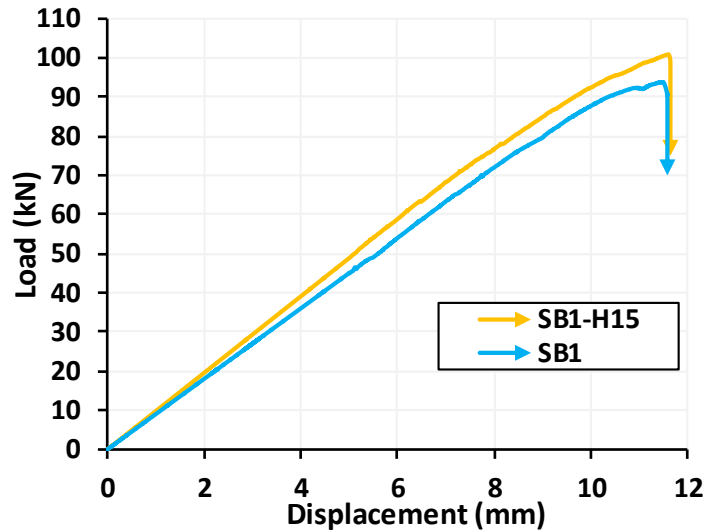


Figure 3.8 Load- displacement responses of specimens SB1-Control and SB1-H15

3.2.5. Conclusions of the Preliminary Study

Results of the first two tested specimens revealed that the mode of failure and the load-deflection response of interior slab-column connections strengthened by hemp fabric sheets bonded to the tension face were independent of the type of epoxy used to bond the sheets. Therefore, it was decided to use Sikdur-330 in the research program. Furthermore, the experimental findings of the other two specimens showed that HFRP fabric sheets improved the ultimate shear capacity as well as increased the stiffness of the strengthened interior slab-column connection relative to the control specimen, which paved the way to launching the bigger scale study with different test parameters needed to understand better the behavior of the HFRP fabric sheets as strengthening material for interior slab-column connections.

3.3. Part Two: Full-Scale Experimental Program

Twenty-four small-scale interior reinforced concrete 670x670 mm slab-column connection specimens, each with a 100x100 mm center column stub extending 150 mm from the slab's top surface and 50 mm from the bottom surface, were prepared for

testing by using the MTS Universal Testing machine. A 3D schematic view of the test specimen is shown in **Figure 3.9**.

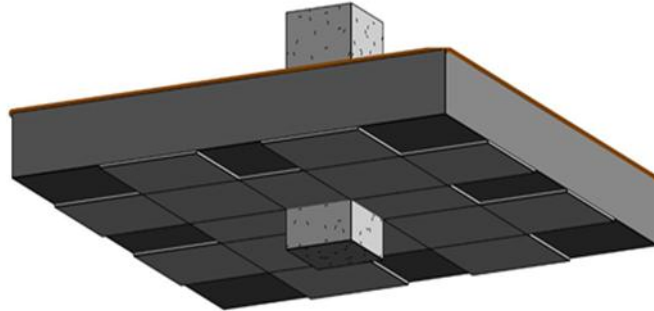


Figure 3.9 Slab-column connection 3D view

3.3.1. Test Variables

The main test variables in this study are the slab thickness (55 or 75 mm), the ratio of steel reinforcement (1% or 1.5%), width of hemp fiber fabric sheet (100, 150, or 200 mm), the number of layers of the HFRP sheets (one or two layers), and the location of hemp strips (adjacent to the column or offset by $1.5d$ from the face of the column). In order to make a comparison between the effect of HFRP sheets and CFRP sheets, 4 of the 24 specimens are strengthened by 150 mm wide CFRP sheets.

The 24 specimens are divided into four groups (SA1, SA2, SB1, and SB2) where SA and SB designate the two slab thicknesses: 55 and 75 mm, respectively, and the numbers 1 and 2 refer to the reinforcement ratio: 1 for 1% and 2 for 1.5%. The test variables are listed in **Table 3.4**. Each specimen is identified by a 3-part notation system. The first part is SA1 or SA2 or SB1 or SB2. The second part refers to the type of confinement (H for hemp fabric and F for CFRP) and the confinement sheet's width (10 or 15 or 20 cm). The number in parenthesis at the end of the notation, if it exists, implies two layers of confinement sheets. The third part of the notation refers to the

location of the HFRP fabric strips relative to the column side: A for adjacent and O for offset by 1.5d from the column's face.

Table 3.4 Test variables

Series	Specimen Designation	Slab Thickness (mm)	Steel Ratio	FRP Type	FRP Width (cm)	No. of Layers	Strengthening Configuration
SA1	SA1	55	1%	-	-	-	-
	SA1-H10-A	55	1%	HFRP	10 cm	1	Adjacent
	SA1-H10-O	55	1%	HFRP	10 cm	1	Offset
	SA1-H15-A	55	1%	HFRP	15 cm	1	Adjacent
	SA1-H15-O	55	1%	HFRP	15 cm	1	Offset
	SA1-H20-A	55	1%	HFRP	20 cm	1	Adjacent
	SA1-F15-A	55	1%	CFRP	15 cm	1	Adjacent
SA2	SA2	55	1.5%	-	-	-	-
	SA2-H15-A	55	1.5%	HFRP	15 cm	1	Adjacent
	SA2-H15-O	55	1.5%	HFRP	15 cm	1	Offset
	SA2-H20-A	55	1.5%	HFRP	20 cm		Adjacent
	SA2-F15-A	55	1.5%	CFRP	15 cm	1	Adjacent
SB1	SB1	75	1%	-	-	-	-
	SB1-H15-A	75	1%	HFRP	15 cm	1	Adjacent
	SB1-H15-O	75	1%	HFRP	15 cm	1	Offset
	SB1-H20-A	75	1%	HFRP	20 cm	1	Adjacent
	SB1-H15(2)-A	75	1%	HFRP	15 cm	2	Adjacent
	SB1-F15-A	75	1%	CFRP	15 cm	1	Adjacent
SB2	SB2	75	1.5%	-	-	-	-
	SB2-H15-A	75	1.5%	HFRP	15 cm	1	Adjacent
	SB2-H15-O	75	1.5%	HFRP	15 cm	1	Offset
	SB2-H20-A	75	1.5%	HFRP	20 cm	1	Adjacent
	SB2-H15(2)-A	75	1.5%	HFRP	15 cm	2	Adjacent
	SB2-F15-A	75	1.5%	CFRP	15cm	1	Adjacent

3.3.2. Materials

3.3.2.1. Concrete

Normal weight concrete was used throughout the experimental program. The concrete mix consisted of Portland cement Type I, sand, and well-graded crushed limestone aggregates with a maximum size of 10 mm. The intended concrete compressive strength for all specimens was 35 MPa. The proportions by weight of cement to sand to coarse aggregates were 0.32:0.5:1.0 with a water-cement ratio of around 0.5. A superplasticizer dosage of 0.4% by weight of cement was added to increase the concrete mix's consistency. The superplasticizer conformed to ASTM C 494 (ASTM C494 2015). The batching weights were presented in **Table 3.1**. The actual concrete compression strength of each mix was determined by testing 150x300 mm standard cylinders according to ASTM C39 (ASTM C39 2010). **Figure 3.10** shows the test setup of the compression test of a concrete cylinder.



Figure 3.10 Test setup of the compression test of a concrete cylinder

3.3.2.2. Reinforcing Steel

All specimens in groups SA1 and SA2 of 55 mm thick slabs were reinforced using 8 mm Grade 60 deformed bars in each direction, 5 bars for SA1 (1% reinforcement ratio), and 7 bars for SA2 (1.5% reinforcement ratio). On the other hand,

the reinforcement in groups SB1 and SB2 of 75 mm thick specimens consisted of 10 mm Grade 60 deformed bars in each direction, 5 bars for SB1 (1% reinforcement ratio), and 7 bars for SB2 (1.5% reinforcement ratio). The average effective depth to the two reinforcement layers' center was 37 mm for the SA1 and SA2 specimens and 55 mm for the SB1 and SB2 specimens. Four deformed vertical bars were placed at the column stub's corners, 8 mm diameter for the SA specimens and 10 mm for the SB specimens. Along all slab sides, a clear concrete cover of 10 mm was maintained. **Figure 3.11** shows the typical dimensions and steel reinforcement layout of the test specimens. Two coupons of each of the two bar sizes used (8 and 10 mm) were tested using the Universal Testing Machine (UTM) to determine the yield strength and the ultimate strength. The values are listed in **Table 3.5**.

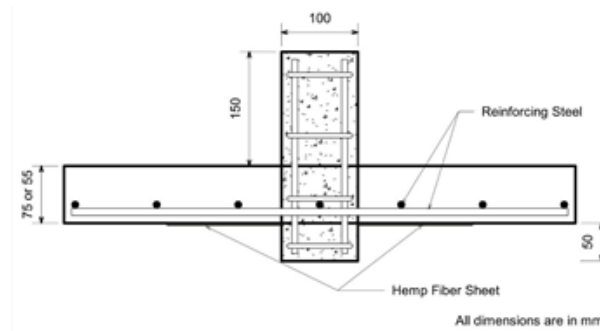


Figure 3.11 Dimensions and reinforcement details of the slab specimen

Table 3.5 Mechanical characteristics of the steel bars

Properties		Bar 8 (mm)	Bar 10 (mm)
Yield stress (MPa)	f_y	570	570
Ultimate stress (MPa)	f_u	640	640

3.3.2.3. HFRP Fabric Sheet

Commercial bi-directional HFRP fabric sheets were used to strengthen the slab-column connections. The fabric was supplied in a 1,500 mm-wide roll and was cut into

designated sizes to conduct this study. The tensile properties of the material used could be determined by performing a tensile test of three HFEP strips. 25x300 mm strips were impregnated in epoxy resin and left to dry after removing excess epoxy (**Figure 3.12**). Then the strips were allowed to cure for two weeks before testing.

The tensile test for the HFRP fabric strip was conducted according to D3822/D3822M-14, (2020) at a constant rate of extension of 1 mm/min. This rate was chosen to be the same rate used during testing of the slab-column specimens using the MTS machine. Clamps and flat jaws with a gauge length of 200 mm were used to grip the strips and minimize their slippage. The average thickness of the strips as measured before performing the tensile test was 1.2 mm. **Figure 3.13** shows the test setup of the performed tensile test. When the tensile load was applied to the HFRP fabric strips, fiber elongation increased as the load increased until peak stress of 30 MPa was reached, at which the strips exhibited a sudden brittle failure (**Figure 3.14**). The stress-strain curve shown in **Figure 3.15** is almost linear up to a stress level of around 28 MPa. The modulus of elasticity is 3.7 GPa, and the ultimate strain is 0.035 mm/mm.



Figure 3.12 Preparation of the HFRP fabric strips for tensile testing



Figure 3.13 Tensile test setup of the HFRP fabric strips



Figure 3.14 Mode of failure of the HFRP fabric strip

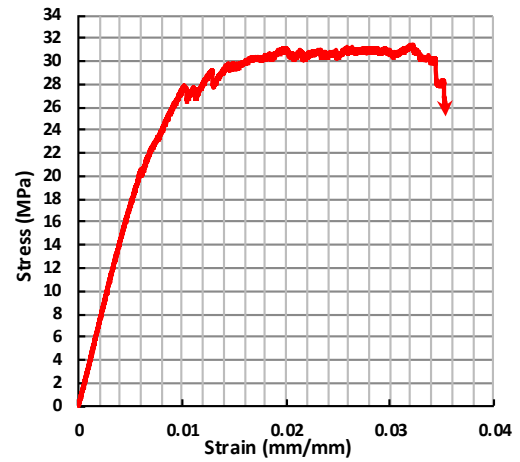


Figure 3.15 Stress-strain curve of the tested HFRP fabric strip

3.3.2.4. Carbon Fiber Reinforced Polymer (CFRP) Sheet

The CFRP confinement sheets used in 4 out of the 24 specimens were SikaWrap-230 C. **Table 3.6** shows the properties of the used CFRP sheets.

Table 3.6 The properties of the CFRP SikaWrap-230 C

Property		Values
Dry Fiber Properties	Dry Fiber Density	1.82 g/cm ³
	Dry Fiber Thickness	0.129 mm (based on fiber content)
	Dry Fiber Tensile Strength	4 000 N/mm ² (ISO 10618)
	Dry Fiber Modulus of Elasticity in Tension	230 000 N/mm ² (ISO 10618)
	Dry Fiber Elongation at Break	1.7% (ISO 10618)
Laminate Properties	Laminate thickness	0.129 mm
	Laminate Nominal Cross Section	129 mm ² per m width
	Laminate Tensile Strength	3 500 N/mm ²
System Structure	Concrete substrate adhesive primer- Sikadur-330.	
	Impregnating/ laminating resin - Sikadur-330.	
	Structural strengthening fabric - SikaWrap-230C.	

3.3.2.5. The Adhesive Sikadur-330

The adhesive Sikadur-330 is a 2-component, thixotropic epoxy-based impregnating resin, and adhesive used to bond the strengthening material (hemp fabric or CFRP sheets) to the test specimens. Sikadur-330, which is Sika Company's product, consists of two components where the mix ratio of Component A to Component B by weight is 4 to 1. The mechanical properties of the epoxy, as provided by the supplier, were shown in **Table 3.3**.

3.3.3. Fabrication of the Slab-Column Specimen

3.3.3.1. Formwork

The slab steel bars were cut into the required length and tied together in the laboratory. Then, the four-column bars were tied together by four ties and placed in the middle of two-way slab reinforcement. Finally, the whole reinforcement cage was installed in the wood form while maintaining a clear concrete cover of 10 mm by installing proper spacers (**Figure 3.16**).



Figure 3.16 View of the formwork before concrete casting

3.3.3.2. Concrete Casting

Concrete batching was done using a small mixer in the laboratory (**Figure 3.17**). Each batch was used to cast two specimens and six concrete cylinders. The concrete was placed in the form and adequately consolidated. After that, the concrete surface was leveled off, a plywood cover was installed to be able to cast the column stub (**Figures 3.18 and 3.19**). Finally, the specimens were left in the curing room for 28 days (**Figure 3.20**).



Figure 3.17 Concrete batching

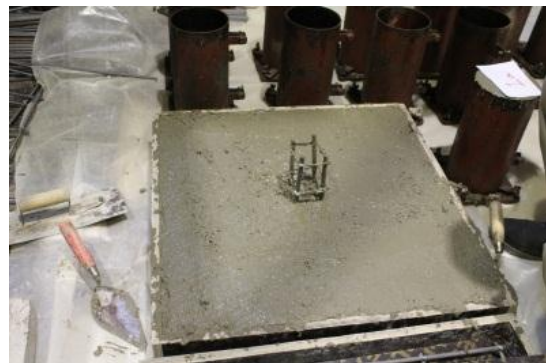


Figure 3.18 Levelling of the cast slab

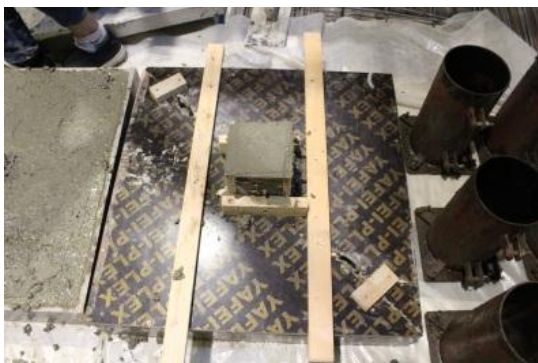


Figure 3.19 Casting the column stub after placing a plywood piece above the cast slab



Figure 3.20 View of the specimens placed in the curing room

3.3.3.3. Installation of the HFRP Fabric Sheets

First, the HFRP fabric sheets were cut into the desired length and width. Second, all the dust and impurities on the slab-column specimen's tension side were removed using abrasive sheets and a vacuum machine. Before installing the HFRP fabric sheet,

two components of the Sikdur-330 epoxy resin were mixed according to the manufactured company's user manual (**Figure 3.21**). Then a thin layer of epoxy was applied at the proper location (**Figure 3.22**), while the sheet was saturated with epoxy resin (**Figure 3.23**) and laid above the epoxy layer (**Figure 3.24**). A rubber roller was passed on the installed fabric sheets to make sure no air bubbles were trapped between the fabric, epoxy resin, and the concrete surface (**Figure 3.25**). All the HFRP fabric sheets were installed during the same day and kept one week as curing time before the specimens were tested. **Figure 3.26** shows the specimen after installing the hemp fabric sheets.



Figure 3.21 Mixing the two components of Sikadur-330



Figure 3.22 Applying the epoxy layer before installing the HFRP sheet



Figure 3.23 Saturation of the HFRP sheet with epoxy



Figure 3.24 Installing the HFRP sheet above the epoxy layer



Figure 3.25 Applying a rubber roller on the HFRP sheet

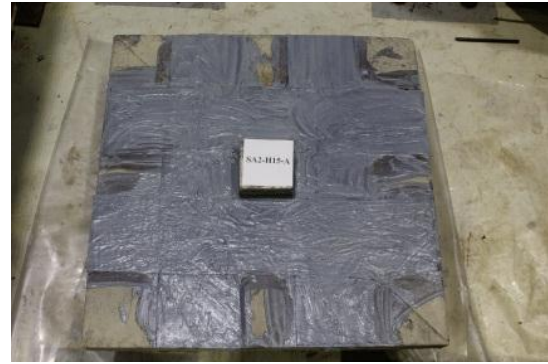


Figure 3.26 View of the strengthened specimen

3.3.4. Testing Program

3.3.4.1. Instrumentation

Test measurements included the magnitude of the applied load, deflection of the slab at the column location, and strain in the HFRP or CFRP strips. The instrumentation of the test setup consisted of various Linear Variable Differential Transducers (LVDT's) to measure deflections and a computerized data acquisition system. Two LVDT's were placed on steel plates on opposite sides of the tested specimen, as shown in **Figure 3.3**. The LVDT's deflection readings were averaged to obtain the displacement at the center of the slab. A third LVDT was placed on one of the slab specimens' corners to detect the uplifting value during testing. Two strain gauges were installed, one at mid-length of each of two perpendicular strengthening strips, to measure the strain in the HFRP or CFRP strips, as shown in **Figure 3.27**. A computerized data acquisition system was monitored the data, including the applied load, the LVDT's, and strain gauges' readings.

3.3.4.2. Test Setup

All specimens were loaded centrally through the column stub with monotonically increased load until failure using the MTS Universal Testing machine

(**Figure 3.28**). The test was displacement controlled, where the load was applied at an approximate average rate of 1 mm/min. The specimens were mounted on a steel frame with 40 mm wide pedestals on all four sides; the corners of the slab were free to lift when the load was applied. A steel cap with a rubber heading was placed on the column stub's top to distribute the load monolithically so, the column would not fail before the slab.

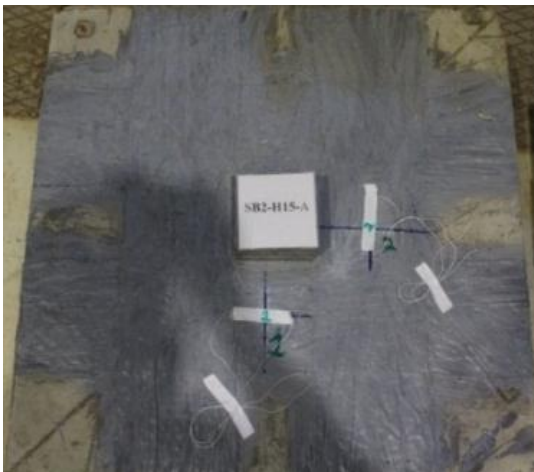


Figure 3.27 Locations of the two strain gauges



Figure 3.28 Test setup of the specimen

CHAPTER 4

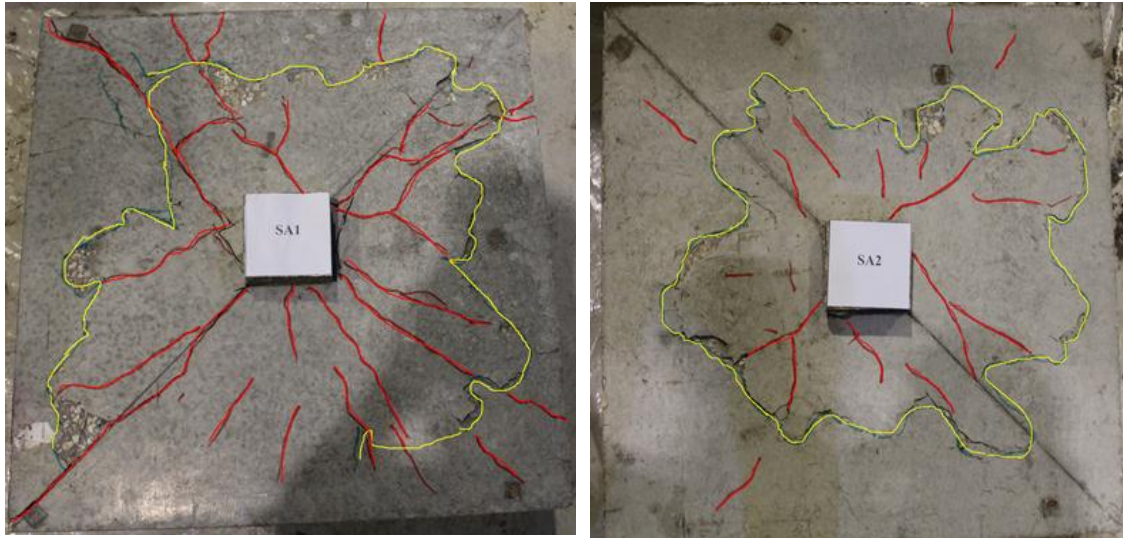
DISCUSSION OF TEST RESULTS AND ANALYSIS

4.1. Introduction

This chapter aims to describe the mode of failure and to analyze the 24 tested slab-column specimens' experimental results. The effect of each test variable adopted in this study will be investigated in terms of the mode of failure, the ultimate shear capacity, and the load-deflection response of the tested specimens.

4.2. Mode of Failure

The mode of failure of the tested specimens in this study can be classified into two different types: pure punching shear failure and combined punching-flexural failure. All specimens showed clear evidence of punching shear failure except the five specimens SA1, SA1-H10-A, SA1-H10-O, SA1-H20-A, and SA1-F15-A, experienced combined punching-flexural failure. Those five specimens developed both flexural and punching shear cracks on the tension side of the slab, where flexural yield lines started at the corners of the column stub and propagated towards the edges of the slab, combined with punching shear cracks that were characterized by one major circumferential crack away from the column face, as can be seen in **Figure 4.1a**. Failure of the remaining specimens was identified as a two-way shear failure. Shear failure in these specimens was detected by observing inclined cracks forming at a distance away from the column stub's perimeter in the slab tension face, as shown in **Figure 4.1b**, followed by a sudden punching of the column stub through the slab at the compression face.

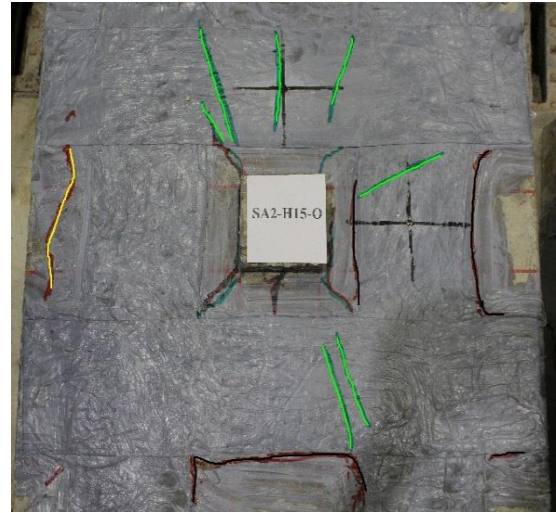
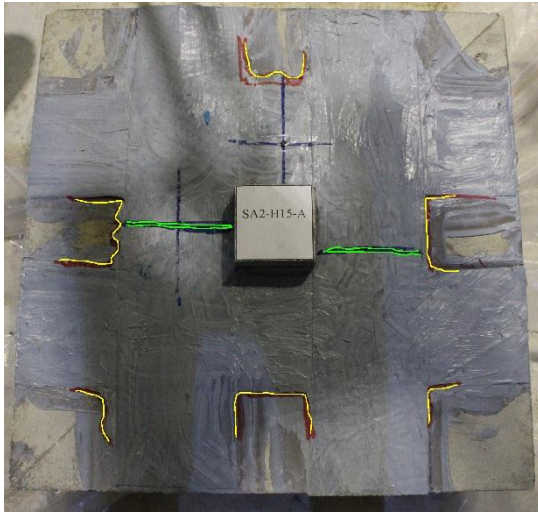


(a) Combined punching-flexural failure

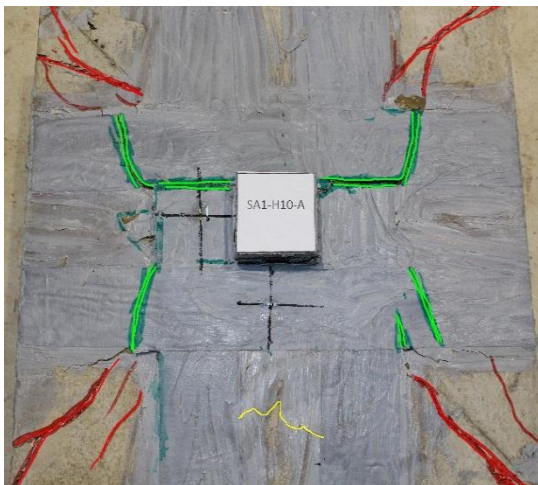
(b) Pure punching shear failure

Figure 4.1 Typical crack patterns at failure

Failure of most specimens strengthened by HFRP sheets was preceded by tearing or breaking of the HFRP sheets in the critical maximum moment region (at mid-length of the HFRP sheets), and bond failure between the HFRP sheets and the concrete surface was found along the major cracks of the specimens, as shown in **Figure 4.2a**. However, the HFRP sheets' debonding failure was clearly observed in specimen SA1-H10-A, which was evident from the easily peeling off of the HFRP sheets from the concrete surface after the test was performed, as can be seen in **Figures 4.2b** and **4.2c**. Failure of specimen SA1-H20-A was accompanied by breaking of HFRP sheets not only in its mid-length but also two of the sheets broke near the supports (**Figure 4.2d**). Furthermore, the two specimens SB1-H15(2)-A and SB2-H15(2)-A experienced the same failure mode as the majority of specimens strengthened by HFRP. However, the two HFRP layers were broken, as shown in **Figure 4.2e**.



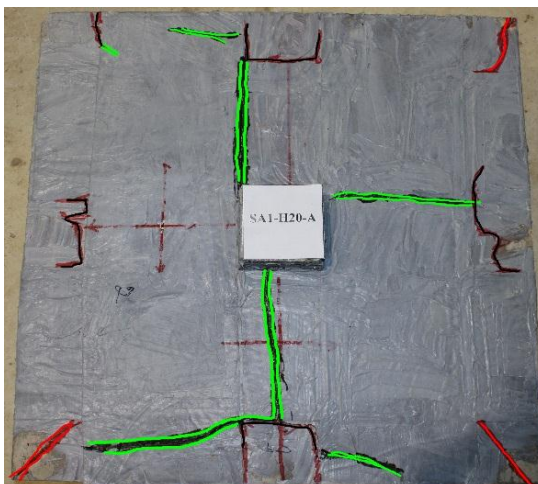
(a) Typical failure for HFRP sheets



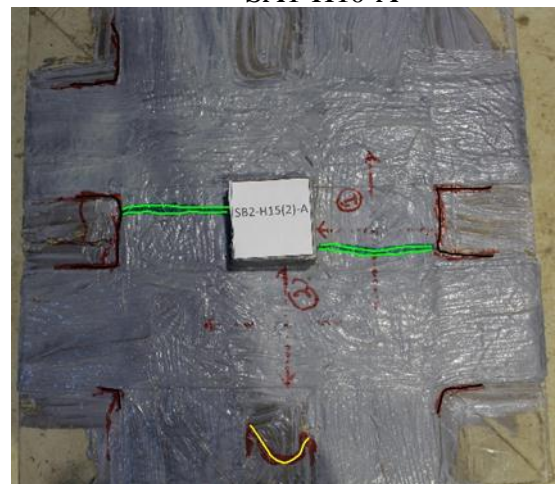
(b) Failure of specimen SA1-H10-A



(c) Peeling off of the HFRP sheets in SA1-H10-A



(d) Failure of specimen SA1-H20-A



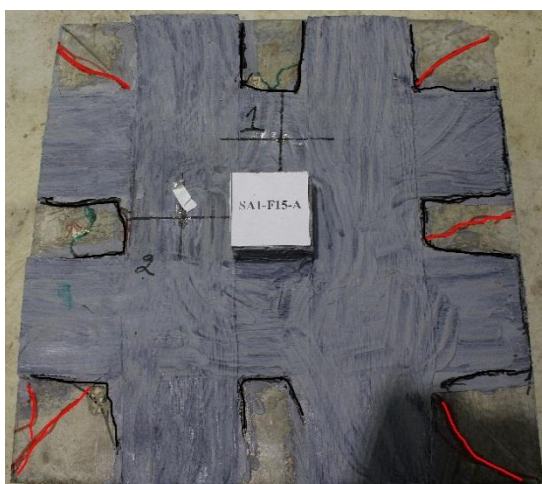
(e) Failure of double layers specimen SB2-H15(2)-A

Figure 4.2 Failure of specimens confined and strengthened by HFRP sheets

On the other hand, none of the CFRP strengthened specimens experienced a break or tension fracture of the CFRP sheets. However, due to the fact that CFRP sheets have no resistance in the transverse direction, a detachment of these sheets was observed on either side of the punching shear cracks plane, as shown in **Figure 4.3a**. A delamination failure of CFRP sheets was observed in specimen SA1-F15-A, where the whole CFRP sheets system could be effortlessly removed from the slab surface after the specimen's failure occurred (**Figures 4.3b** and **4.3c**).



(a) Typical failure of specimens strengthened by CFRP



(b) Failure of specimen SA1-F15-A

(c) Debonding of CFRP sheets in SA1-F15-A

Figure 4.3 Failure of specimens confined and strengthened by CFRP sheets

The average distance from the face of the column to the punching shear failure plane at the tension face of the specimen was 2.9h to 3.8h in series SA1 and SA2, and between 2h to 3.2h for specimens in series SB1 and SB2, where h is the slab thickness. It was noticed that the presence of the HFRP or CFRP confinement sheets did not affect the position of the shear failure plane; Propagation of the shear cracks away from the column stub in the slab tension face was almost the same for control and confined specimens.

It should be mentioned that specimens which experienced pure punching shear failure failed in a brittle manner. When the tested specimen reached its maximum shear capacity, a sudden punching of the column stub through the slab occurred accompanied by a loud noise. On the other hand, specimens that experienced combined punching-flexural failure failed in a ductile manner by forming yield lines through slab thickness before the column punched through the slab. As the applied load was increased, a soft sound of concrete cracks was heard, followed by a loud noise when punching occurred.

4.3. Test Results and Analysis

Test results of all 24 specimens are presented in **Table 4.1**. The results include f'_c at the day of testing; the ultimate load normalized at a common f'_c of 35 MPa by multiplying the actual experimental value by $\sqrt{35/f'_c}$, percentage change (increase or decrease) of the ultimate load relative to the control specimen in the series, deflection at ultimate load, fracture energy calculated as the area under the load-deflection curve, energy ductility index computed as the fracture energy of the specimen divided by the fracture energy of the control specimen in the same series, the initial stiffness or slope

of the load-deflection curve, and the percentage change (increase or decrease) in the initial stiffness relative to the control specimen in the same series.

In the following subsections, the effect of the confining sheet width, location of the sheet relative to the column, and the type of the sheet, whether it is HFRP or CFRP, on the test results and load-deflection behavior will be presented and analyzed for each of the four series tested: SA1, SA2, SB1, and SB2. It is important to note that the specimens' load-deflection curves were also normalized at a common f'_c of 35 MPa by multiplying the actual experimental load value at each deflection by $\sqrt{35/f'_c}$.

4.3.1. Series SA1

The seven specimens in Series SA1 have a slab thickness of 55 mm and a steel reinforcement ratio of 1% resulting in five 8 mm bars in each direction with an average effective depth d of 37 mm. The span to depth ratio is 25. With the exception of specimens SA1-H15-A and SA1-H15-O which experienced pure punching shear failure, all other five specimens in the series had combined punching-flexural failure.

4.3.1.1. Influence of the Width of HFRP Sheets

Figure 4.4 presents a comparison between the normalized load-deflection curves for four specimens in Series SA1 confined with HFRP sheets of different widths. Specimen SA1-H15-A had a pure punching shear failure, whereas the other three specimens had combined punching-flexural failure.

Apparently, the shape of load-deflection curves can be used to distinguish the failure type of the specimens. All specimens displayed an almost bilinear behavior up to the ultimate load that can be divided into two phases: the first phase of response is

characterized by the initial stiffness of the uncracked slab at the early loading stage, and the second phase can be identified by a reduction in the stiffness due to the development of tensile flexural cracks. After the ultimate load is reached, specimen SA1-H15-A, which experienced pure punching shear failure, had a very sharp drop in load. On the other hand, the other three specimens that had combined punching-flexural failure experienced relatively more considerable deflections in the post-ultimate stage due to the reinforcing bars' yielding before the occurrence of the punching shear failure, which resulted in a sharp drop of the load.

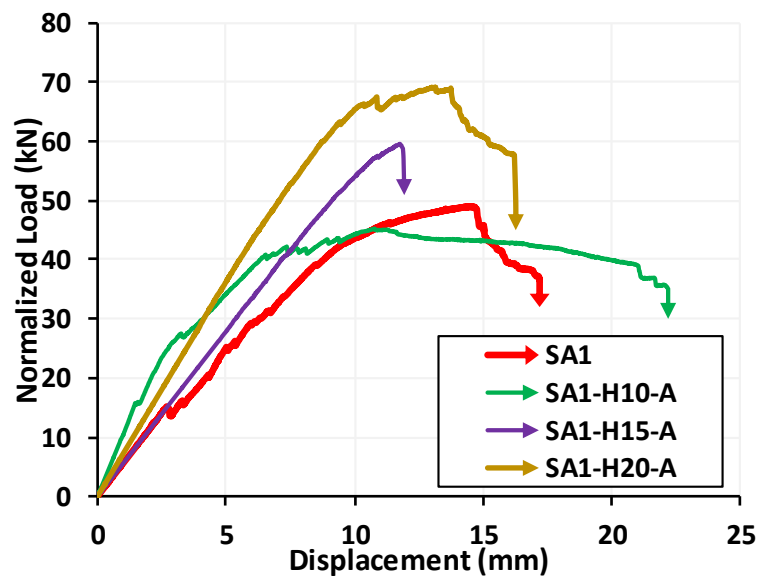


Figure 4.4 Load-deflection curves of specimens with different HFRP sheet width, Series SA1

Table 4.1 Summary of the test results

Series	Specimen	f'_c (MPa)	Normalized ultimate load P_U (kN)	Ratio of ultimate loads (%)	Deflection at ultimate load (mm)	Fracture energy (kN-m)	Energy Ductility Index	Initial stiffness (kN/mm)	Stiffness Increase (%)
SA1	SA1*	43.7	49	-	14.58	0.563	-	4.6	-
	SA1-H10-A*	36	45.26	-7.63%	10.78	0.827	1.469	6.62	43.37%
	SA1-H10-O*	36	53.27	8.714%	12.35	0.58	1.03	6.8	47.35%
	SA1-H15-A	36.5	59.6	21.63%	11.763	0.3935	0.7	5.58	20.9%
	SA1-H15-O	36.5	62.94	28.44%	11.84	0.4466	0.79	6.32	37.03%
	SA1-H20-A*	32.4	69.16	41.14%	13.15	0.752	1.34	7.232	56.8%
	SA1-F15-A*	38.3	69.7	42.24%	10.94	0.813	1.44	7.14	54.8%
SA2	SA2	33.5	70.28	-	10.8	0.436	-	7.336	-
	SA2-H15-A	32.4	69.54	-1.05%	11.8	0.48	1.1	7.091	-3.27%
	SA2-H15-O	38	78.72	12%	13	0.61635	1.414	7.0613	-3.7%
	SA2-H20-A	35	74.17	5.54%	13.33	0.613	1.406	7.3	-0.41%
	SA2-F15-A	33.55	79.02	12.4%	10.2	0.455	1.0435	8.5	15.7%
SB1	SB1	33.6	93.57	-	11.8	0.711	-	9.81	-
	SB1-H15-A	36.5	98.9	5.7%	10.1	0.566	0.796	10.742	9.5%
	SB1-H15-O	30	108.25	15.7%	11.6	0.729	1.03	11.324	15.4%
	SB1-H20-A	36.5	100.35	7.25%	10.16	0.597	0.84	11.7	19.25%
	SB1-H15(2)-A	35	102.43	9.47%	11.32	0.6972	0.98	11.48	17%
	SB1-F15-A	41.5	117.01	25%	11.072	0.7166	1	10.89	11.12%
SB2	SB2	34.7	117.26	-	10.107	0.6566	-	12.87	-
	SB2-H15-A	35	132.65	13.12%	12.1	0.9	1.37	12.4	-3.7%
	SB2-H15-O	34.7	136.89	16.74%	11.92	0.865	1.32	11.91	-7.4%
	SB2-H20-A	38	133.9	14.2%	12.19	0.97	1.477	12.33	-4.2%
	SB2-H15(2)-A	36.5	129.56	10.49%	11.6	0.888	1.35	13.6	5.7%
	SB2-F15-A	35	140.42	19.75%	10.59	0.81	1.234	13.57	5.44%

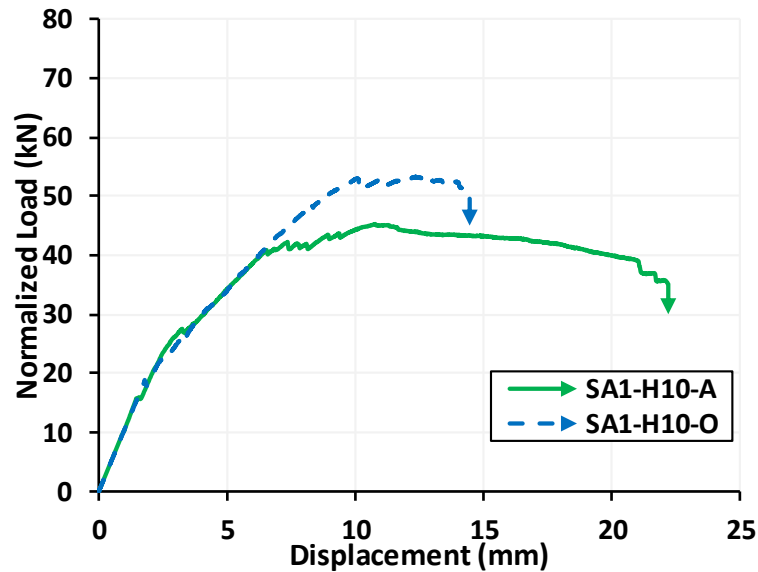
*Specimens SA1, SA1-H10-A, SA1-H10-O, SA1-H20-A, and SA1-F15-A of Series SA1 are the only specimens in the research program which experienced combined punching-flexural failure.

Referring to **Figure 4.4** and the results listed in **Table 4.1**, specimens with 15 and 20 cm wide HFRP sheets had increases of 21.63% and 41.14% in the punching shear strength values relative to the control specimen SA1; this may be attributed to the fact that most of the tensile cracks were covered by the HFRP sheets of these specimens' tension face. The lower capacity of specimen SA1-H10-A relative to SA1 could be explained by the debonding failure of the HFRP sheets that occurred in this specimen, as seen in **Figure 4.2c**. Also, the 10 and 20 cm HFRP sheets' presence increased the fracture energy relative to SA1. The 15 cm HFRP sheet specimen SA1-H15-A had lower fracture energy than SA1 because it experienced pure punching shear failure compared to the combined punching-flexural failure of SA1. Moreover, the strengthened specimens SA1-H10-A, SA1-H15-A, and SA1-H20-A displayed higher initial load-deflection stiffness as compared to the control specimen SA1; the increases were 43.37%, 20.9% and 56.8%, respectively.

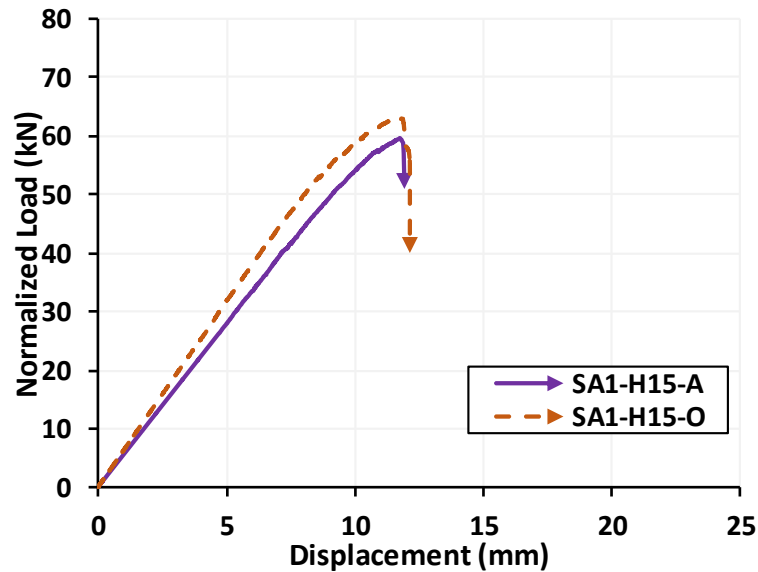
4.3.1.2. Influence of Location of HFRP Sheets

Considering the effect of the location of HFRP sheets relative to the column face in Series SA1, **Figures 4.5a** and **4.5b** display the normalized load-deflection responses of specimens (SA1-H10-A, SA1-H10-O) and specimens (SA1-H15-A, SA1-H15-O), respectively. The HFRP sheets' location did not affect the mode of failure of the strengthened slabs, where both specimens SA1-H10-A and SA1-H10-O failed in combined punching-flexural both specimens SA1-H15-A and SA1-H15-O experienced pure punching failure. As shown in **Figures 4.5a, 4.5b**, and **Table 4.1**, the offset location of the strengthening HFRP sheets at 1.5d from the face of the column led to relatively higher increases in ultimate shear strength than the adjacent location; this can

be explained by the fact that the offset position of the sheets covered the generated major cracks, leading to an increase in the punching shear capacity. Moreover, the sheets' offset location had a positive impact on the initial stiffness of the load-deflection curve, especially for the 15 cm sheets.



(a) SA1-H10-A vs SA1-H10-O



(b) SA1-H15-A vs SA1-H15-O

Figure 4.5 Load-deflection curves of specimens with different location of the HFRP sheet relative to the column face in Series SA1

4.3.1.3. Influence of the Type of Confining Sheet: HFRP versus CFRP

The effect of the type of the confining sheet, HFRP or CFRP, on the load-deflection behavior can be studied by plotting the normalized load-deflection curves of companion specimens identical except for the sheet type: SA1-H15-A and SA1-F15-A (**Figure 4.6**). The CFRP specimen's performance was superior in terms of increase in punching shear capacity and initial load-deflection stiffness compared to the HFRP specimen. The ultimate shear strength and stiffness increases relative to the control specimen SA1 were 42.24% and 54.8% for specimen SA1-F15-A and 21.63% and 20.9% for specimen SA1-H15-A; this is supposedly due to the higher tensile strength and stiffness of the CFRP material as compared with HFRP.

However, when the natural HFRP sheet width increased from 15 to 20 cm, specimen SA1-H20-A exhibited approximately the same performance in load capacity and initial stiffness as specimen SA1-F15-A, despite the difference in mechanical properties of the two materials. This finding could be interpreted by the sheets' failure mode and the amount of concrete area covered by the strengthening material. As was shown in **Figure 4.2d**, the 20 cm HFRP sheets covered most of the tensile cracks in the tested specimen, and the primary reason for the failure of the sheets was tensile rupture, whereas **Figures 4.3b** and **4.3c** clearly show the debonding failure between the CFRP sheet and the concrete surface that occurred in specimen SA1-F15-A.

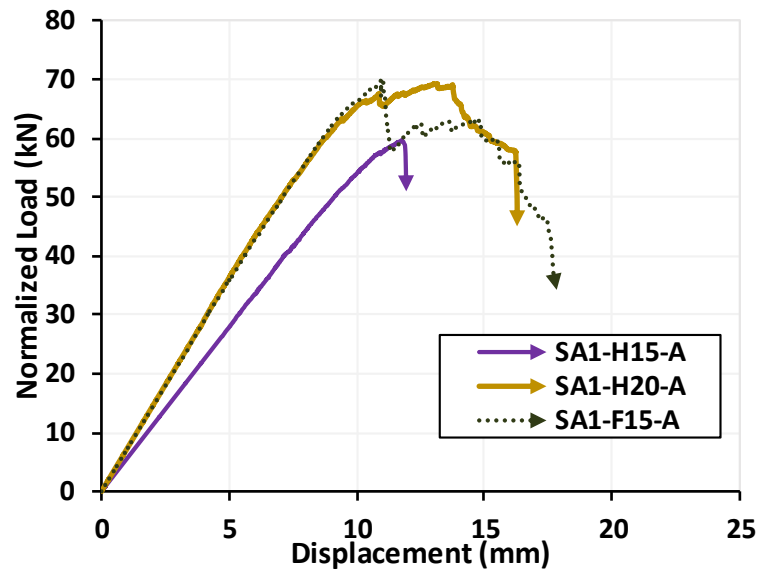


Figure 4.6 Load-deflection curves for specimens SA1-H15-A, SA1-H20-A, and SA1-F15-A

4.3.2. Series SA2

The five specimens in Series SA2 had a similar slab thickness of 55 mm as Series SA1, but the steel reinforcement ratio was increased to 1.5% resulting in seven 8 mm bars in each direction. Like SA1, the average effective depth d was 37 mm, and the span to depth ratio was 25. All specimens in this series experienced pure punching shear failure. Increasing the reinforcement ratio from 1% in SA1 to 1.5% in SA2 led to a significant improvement in the load-deflection history's initial stiffness and improved the ultimate load capacity by an average of 43.43%. Load-deflection curves of the control specimens SA1 and SA2 in both series are shown in **Figure 4.7**. The fracture energy of specimen SA1 was greater than SA2 due to the mode of failure combined with punching and flexural failure for SA1 and pure punching for SA2.

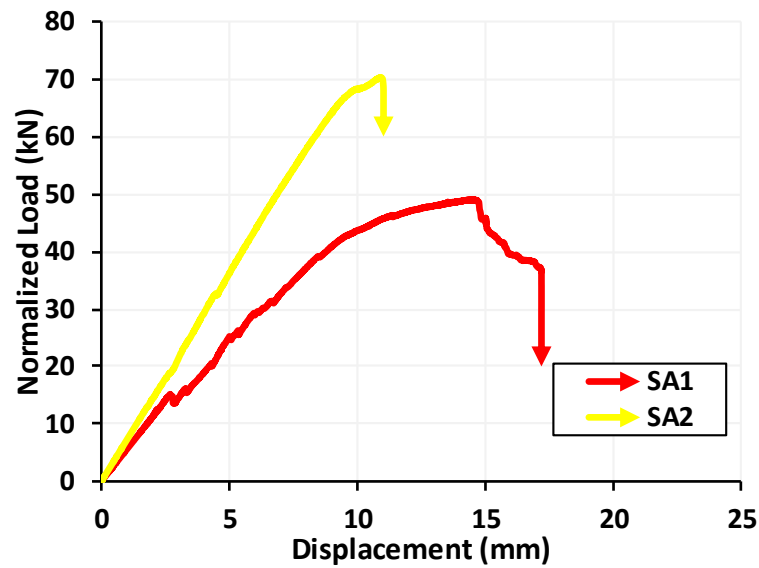


Figure 4.7 Load-deflection curves of the control specimens SA1 and SA2, identical except for the reinforcement ratio

4.3.2.1. Influence of the Width of HFRP Sheets

The normalized load-deflection curves for confined specimens with different widths of HFRP sheets in Series SA2 are shown in **Figure 4.8**. All specimens had a pure punching-shear failure. Unlike Series SA1, the HFRP sheets' width did not affect the initial load-deflection stiffness for the specimens in Series SA2. Referring to **Figure 4.8** and **Table 4.1**, it can be seen that the control specimen and the two other confined specimens, SA2-H15-A and SA2-H20-A, displayed a similar initial stiffness response. However, confinement with 20 cm wide HFRP sheets led to a 5.54% increase in the punching shear load and increased deflection at the ultimate load from 10.8 to 13.33 mm. Therefore, confinement with 20 cm sheets led to a delay in failure and a 41% increase in fracture energy. On the other hand, specimen SA2-H15-A exhibited the same performance as SA2; this may be explained by the HFRP sheets failed before the specimen reach its capacity.

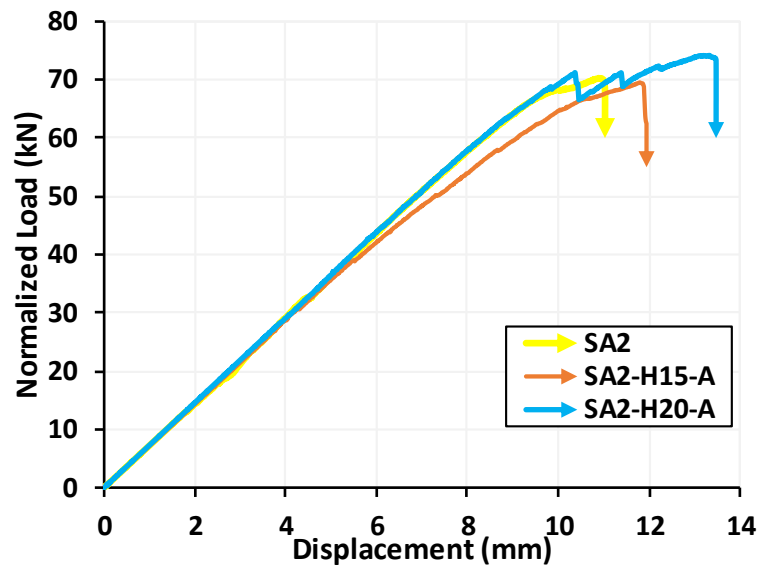


Figure 4.8 Load-deflection curves of specimens with different HFRP sheet width, Series SA2

4.3.2.2. Influence of Location of HFRP Sheets

The normalized load-deflection curves of specimens SA2-H15-A and SA2-H15-O are shown in **Figure 4.9**. It is evident that offsetting the HFRP sheets by 1.5d from the column's face significantly increased the punching shear capacity by around 13%, the deflection at ultimate load, and the energy ductility index by around 28%. Furthermore, both specimens SA2-H15-A and SA2-H15-O showed almost the same stiffness response in load-deflection plots.

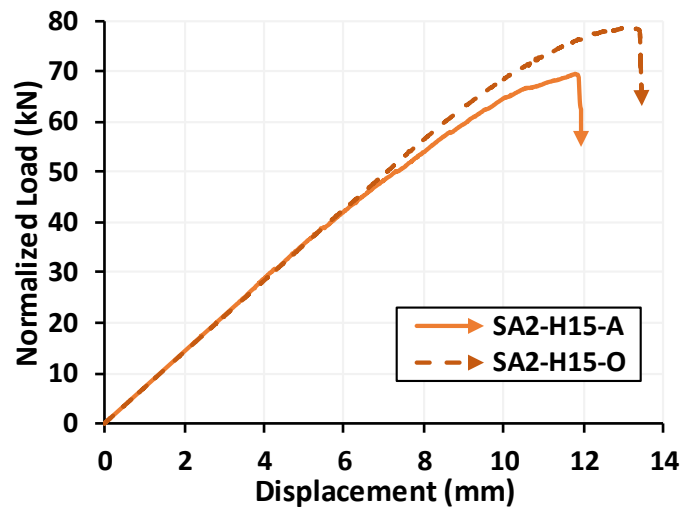


Figure 4.9 Load-deflection curves of specimens with different location of the HFRP sheet relative to the column face in Series SA2

4.3.2.3. Influence of the Type of Confining Sheet: HFRP versus CFRP

To evaluate the possibility of replacing synthetic CFRP with natural HFRP sheets as strengthening material for slab-column connections in Series SA2, **Figure 4.10** displays the three specimens' load-deflection curves SA2-H15-A, SA2-H15-O, and SA21-F15-A. As proved previously in Series SA1, the significant difference between these two materials' mechanical properties contributed to the inferior performance of the HFRP specimen SA2-H15-A relative to the specimen SA21-F15-A, 69.54 kN compared to 79.02 kN. However, when the natural HFRP sheet was applied at the offset location of 1.5d from the column face, specimen SA2-H15-O showed approximately the same ultimate strength of SA2-F15-A, 78.715 kN compared to 79.02 kN. However, the load-deflection response for SA2-F15-A was much stiffer than SA2-H15-O with smaller displacement at ultimate load.

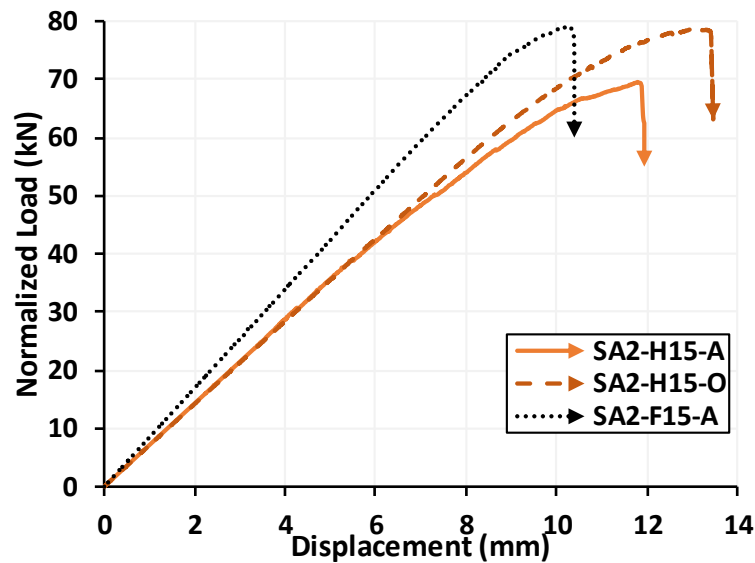


Figure 4.10 Load-deflection curves of specimens SA2-H15-A, SA2-H15-O, and SA2-F15-A

4.3.3. Series SB1

The six specimens in Series SB1 had a slab thickness of 75 mm and a steel reinforcement ratio of 1% resulting in five 10 mm bars in each direction. The average effective depth d was 55 mm, and the span to depth ratio was 18. All specimens in this series had pure punching shear failure. The difference between series SA1 and SB1 was the slab thickness and hence the span to depth ratio, which decreased from 25 in SA1 to 18 in SB1. In general, the increase in slab thickness and hence the reduction in the span to depth ratio led to a significant increase in the load-deflection curves' initial stiffness and to an average increase of 90.9% in the load capacity. The increase in fracture energy of specimens in Series SB1 relative to SA1 is not due to the more ductile post-ultimate load-deflection history, which does not exist due to the pure punching failure of specimens Series SB1, but due to the much greater ultimate load. Load-deflection curves of the control specimens in both series SA1 and SB1 are shown in **Figure 4.11**.

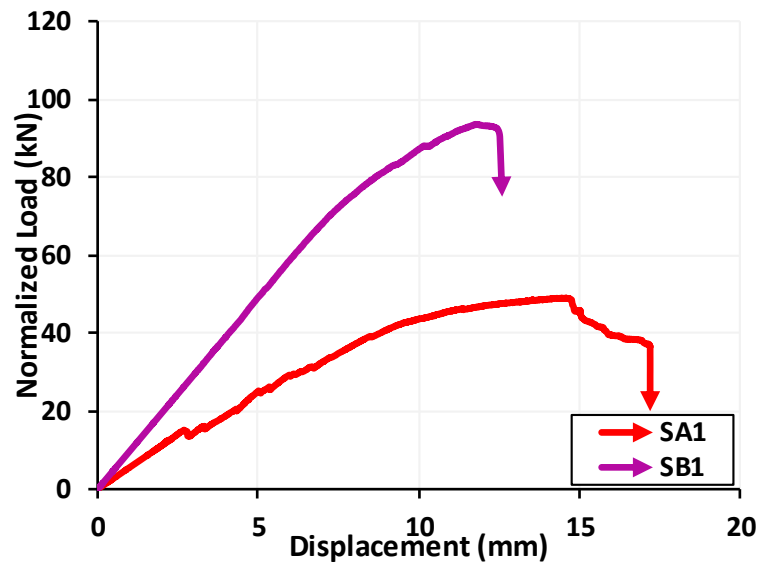


Figure 4.11 Load-deflection curves of the control specimens SA1 and SB1, identical except for the slab thickness and hence the slab to depth ratio

4.3.3.1. Influence of the Width of HFRP Sheets

Figure 4.12 shows the normalized load-deflection curves for the specimens SB1, SB1-H15-A, and SB1-H20-A. Strengthened specimens by HFRP sheets, SB1-H15-A and SB1-H20-A, displayed a higher ultimate punching shear capacity and initial stiffness than the un-strengthened specimen SB1 (refer to **Figure 4.12** and **Table 4.1**). The stiffness increases relative to the control specimen SB1 were 9.5% for specimen SB1-H15-A and 19.25% for specimen SB1-H20-A. It is worth mentioning that both specimens SB1-H15-A and SB1-H20-A had approximately similar ultimate strength with 99 kN and 100.35 kN, respectively, compared to 93.57 kN for SB1. Therefore, the amount of increase in the ultimate shear capacity of specimens in Series SB1, unlike group SA1, was independent of the HFRP sheet's width, 15 and 20 cm.

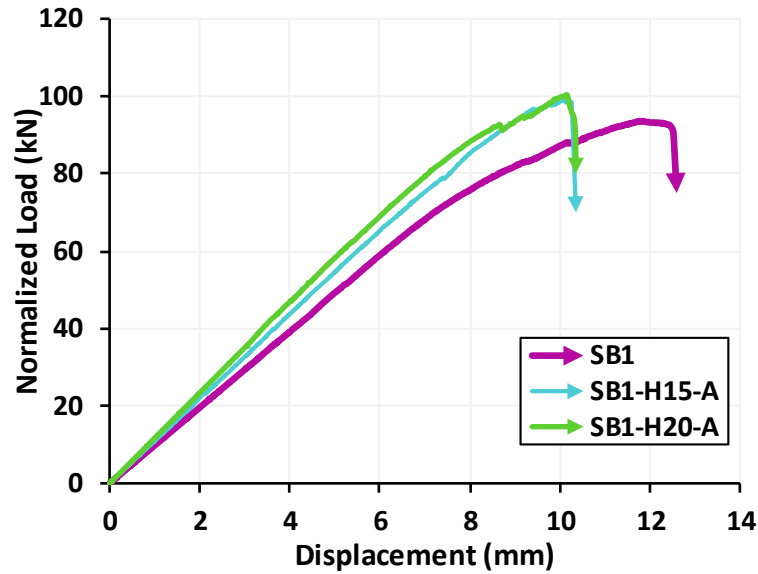


Figure 4.12 Load-deflection curves of specimens with different HFRP sheet width, Series SB1

4.3.3.2. Influence of Location of HFRP Sheets

The effect of the HFRP sheets' location relative to the column face in Series SB1 can be understood by comparing the performance of the two specimens, SB1-H15-A and SB1-H15-O. As shown in **Figure 4.13** and **Table 4.1**, the offset location of the HFRP sheet from the column face produced higher ultimate punching shear capacity than the specimen with adjacent sheets (108.25 compared to 98.9 kN). The increases in normalized shear strength capacity relative to the un-strengthened specimen SB1 were 5.7% for specimen SB1-H15-A and 15.7% for specimen SB1-H15-O. This finding is in line with the results of series SA1 and SA2. Furthermore, both specimens SB1-H15-A and SB1-H15-O exhibited the same initial stiffness in the load-deflection response curve.

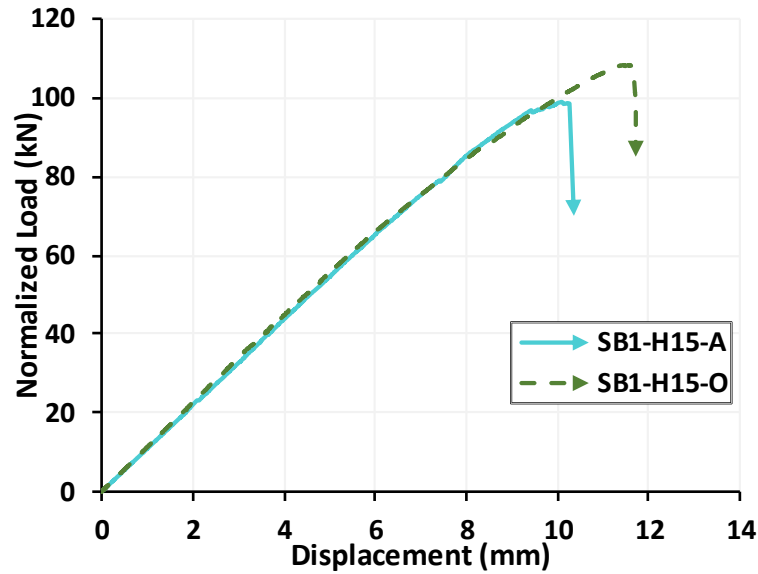


Figure 4.13 Load-deflection curves of specimens with different location of the HFRP sheet relative to the column face in Series SB1

4.3.3.3. Influence of Number of Layers of HFRP Sheets

The effect of doubling the strengthening HFRP sheet was investigated in Series SB1 **Figure 4.14** compares normalized load-deflection curves of specimens SB1-H15-A and SB1-H15(2)-A. The ultimate capacity reached by SB1-H15-A and SB1-H15(2)-A were 98.9 and 102.4 kN, respectively; the values are comparable. It can be clearly seen that both specimens displayed similar response in terms of the mode of failure, initial stiffness, and ultimate shear strength; this could be explained by premature rupture of the second HFRP sheet in specimen SB1-H15(2)-A at a load level of 78 kN, after which the specimen continued to perform as a single layer HFRP specimen (**Figure 4.14**).

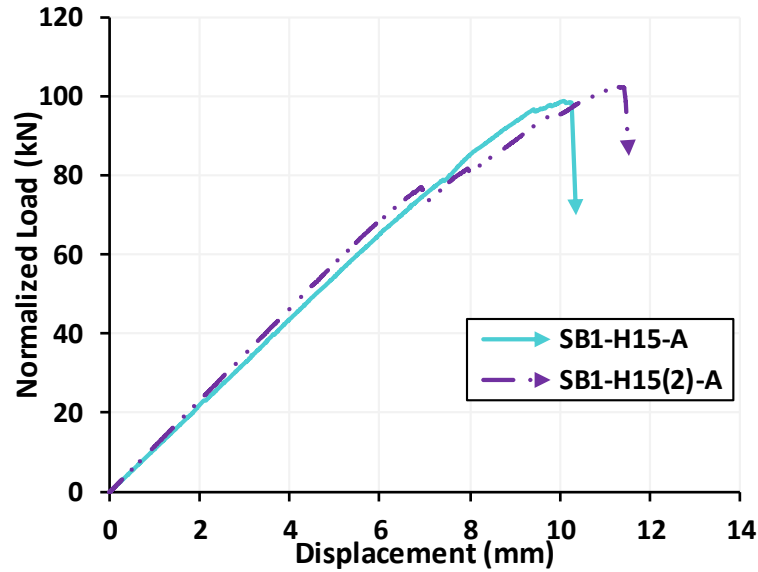


Figure 4.14 Load-deflection curves for specimens SB1-H15-A and SB1-H15(2)-A

4.3.3.4. Influence of the Type of Confining Sheet: HFRP versus CFRP

A comparison of the performance of the load-deflection histories of the tested specimens SB1-H15-A, SB1-H15-O, and SB1-F15-A is presented in **Figure 4.15**. All specimens exhibited the same initial stiffness response. However, the specimen confined by synthetic CFRP, SB1-F15-A, had a relatively greater punching shear capacity (117 kN) than the specimen confined by natural HFRP sheet, SB1-H15-A (98.9 kN). This difference decreased when the HFRP sheets were placed offset from the column face in specimen SB1-H15-O (108.25 kN). This finding confirms the results in Series SA2.

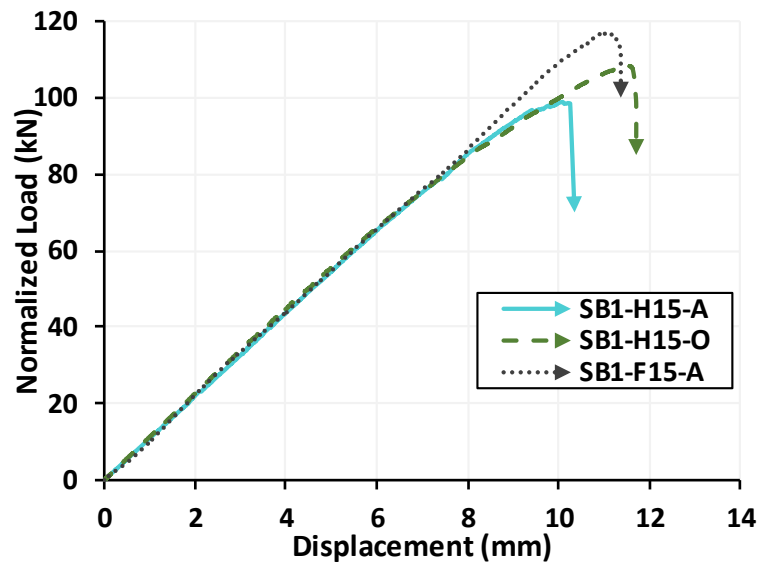


Figure 4.15 Load-deflection curves for specimens SB1-H15-A, SB1-H15-O, and SB1-F15-A

4.3.4. Series SB2

The six specimens in Series SB2 have a slab thickness of 75 mm, an average effective depth d of 55 mm, a span to depth ratio of 18, and a steel reinforcement ratio of 1.5% resulting in seven 10 mm bars in each direction. Like the specimens of Series SB1, all specimens in Series SB2 had pure punching shear failure.

Similar to the difference between series SA1 and SA2, the difference between series SB1 and SB2 was the reinforcement ratio, which was increased from 1.0% in SB1 to 1.5% in SB2. This increase in reinforcement ratio led to a significant increase in load-deflection curves' initial stiffness and increased the ultimate load capacity by an average of 25.3%. Load-deflection curves of the control specimens SB1 and SB2 of both series are shown in **Figure 4.16**.

Also, similar to the difference between series SA1 and SB1, the difference between series SB2 and SA2 was the thickness of the slab, which increased from 55 mm in SA1 to 75 mm in SB2 and hence the slab to depth ratio decreased from 25 in SA2 to 18 in SB2. Specimens in both series SA2 and SB2 experienced pure punching

shear failure. The increase in slab thickness and the reduction in the span to depth ratio of specimens in Series SB2 led to a significant increase in the load-deflection curves' initial stiffness with an average increase of 66.8% in the load capacity relative to specimens in Series SA2. The increase in fracture energy of specimens in Series SB2 relative to SA2 is due to the much greater ultimate load. Load-deflection curves of the control specimens in both series SA2 and SB2 are shown in **Figure 4.17**.

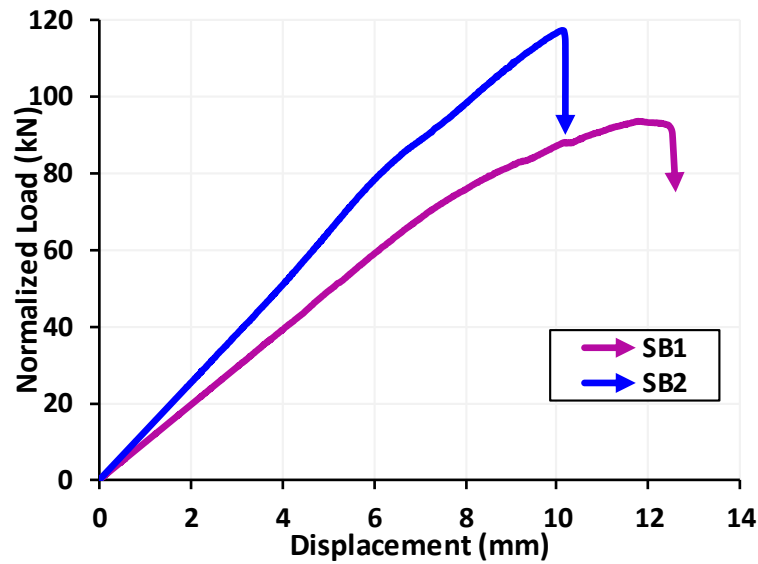


Figure 4.16 Load-deflection curves of the control specimens SB1 and SB2, identical except for the reinforcement ratio

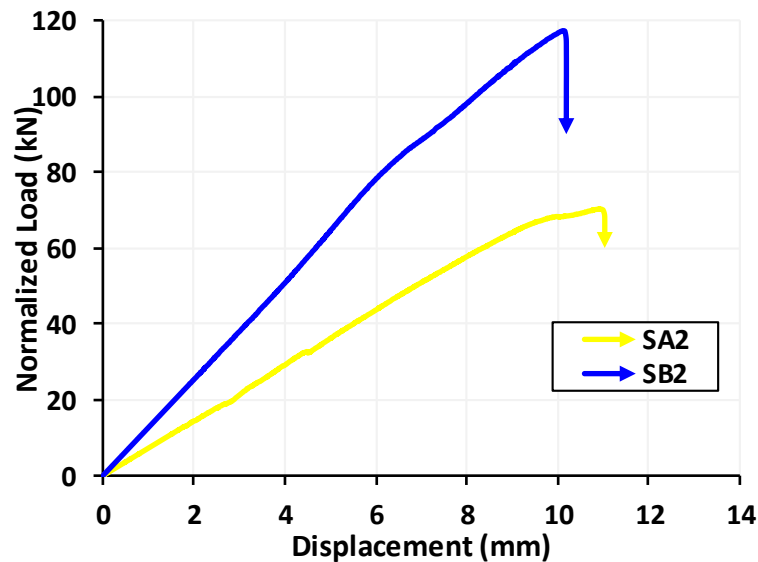


Figure 4.17 Load-deflection curves of specimens SA2 and SB2, identical except for the slab thickness and hence the slab to depth ratio

4.3.4.1. Influence of the Width of HFRP Sheets

Referring to **Figure 4.18** and the results listed in **Table 4.1**, strengthening the slab specimen with 15 or 20 cm wide HFRP sheets led to a very similar performance in initial stiffness and ultimate load capacity. Both specimens SB2-H15-A and SB1-H20-A had almost the same percentage of increase in punching shear capacity relative to the control specimen SB2, 14%. A similar trend was also observed in Series SB1. Although HFRP sheets did not increase the fracture energy of strengthened specimens in Series SB1, the sheets did have a positive impact on the energy ductility index of the strengthened specimens in Series SB2.

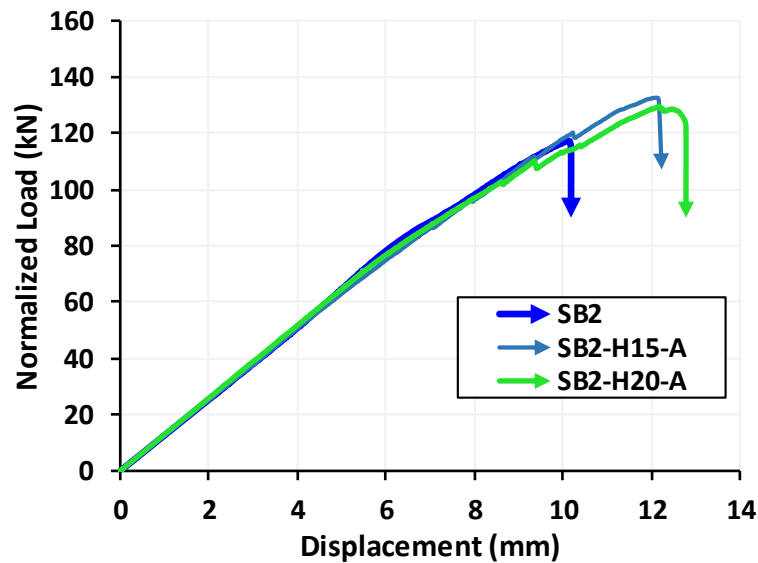


Figure 4.18 Load-deflection curves of specimens with different HFRP sheet width, Series SB2

4.3.4.2. Influence of Location of HFRP Sheets

Referring to **Figure 4.19** and **Table 4.1**, it is clear that the location of the HFRP sheet adjacent or offset from the face of the column did not significantly affect the load-deflection behavior or the ultimate shear load capacity in Series SB2. The ultimate values of the two specimens SB2-H15-A and SB2-H15-O were 132.65 and 136.89 kN,

respectively; the increases relative to the un-strengthened specimen SB2 were 13.12% and 16.74%, respectively.

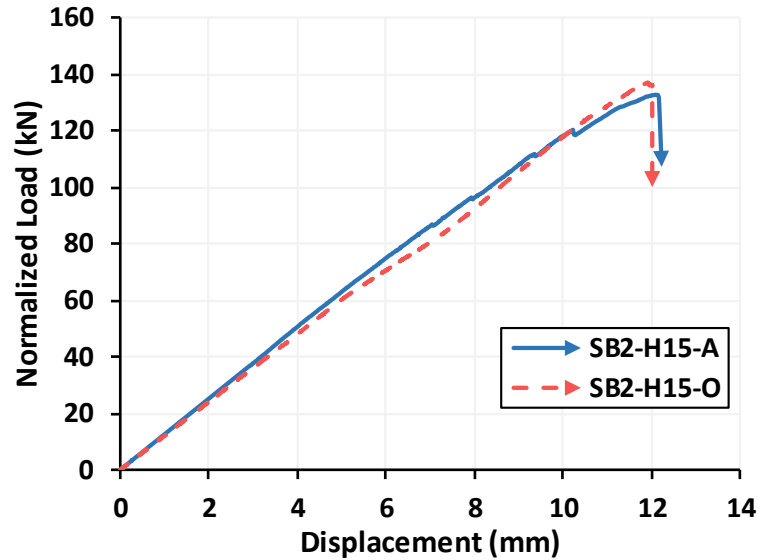


Figure 4.19 Load-deflection curves of specimens with different location of the HFRP sheet relative to the column face in Series SB2

4.3.4.3. Influence of Number of Layers of HFRP Sheets

Observations that were made in Section 4.3.3.3 above concerning the use of double HFRP strengthening sheets in Series SB1 are very similar in Series SB2. Load-deflection curves of the two specimens SB2-H15-A and SB2-H15(2)-A, shown in **Figure 4.20**, are very similar, with a slight increase in initial stiffness when using double sheets. Both specimens showed similar increases in ultimate shear capacity relative to the control specimen SB2, 13.12% for one layer and 10.49% for the two layers. A drop in load was observed when the specimen SB2-H15(2)-A reached a load level of around 120 kN, which could be due to the early break of its second HFRP sheet, and then the double-layered specimen showed similar load-deflection behavior as the single one up till failure.

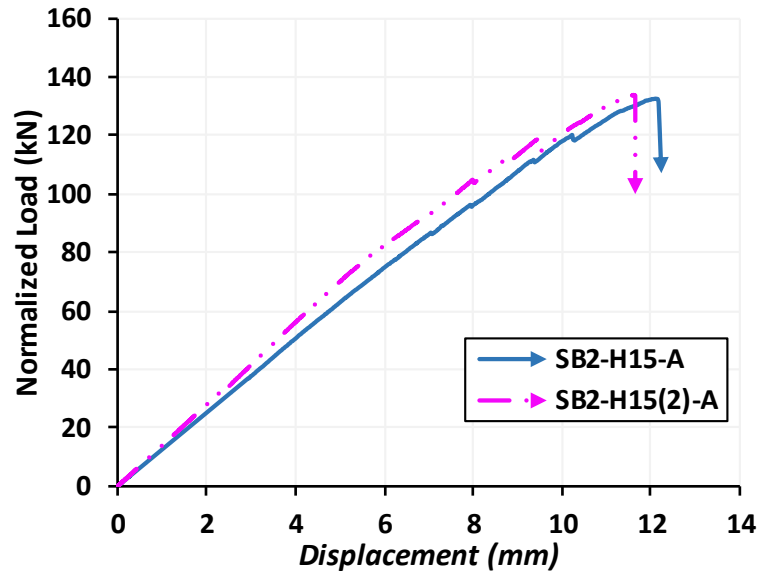


Figure 4.20 Load-deflection curves for specimens SB2-H15-A and SB2-H15(2)-A

4.3.4.4. Influence of the Type of Confining Sheet: HFRP versus CFRP

As is presented in **Figure 4.21** and **Table 4.1**, the specimen confined by synthetic CFRP sheets showed higher stiffness and higher load capacity than specimens confined by natural HFRP sheets. The increases in load capacity relative to the control SB2 for specimens SB2-H15-A, SB2-H15-O, and SB2-F15-A were 13.12, 16.74, and 19.75%, respectively.

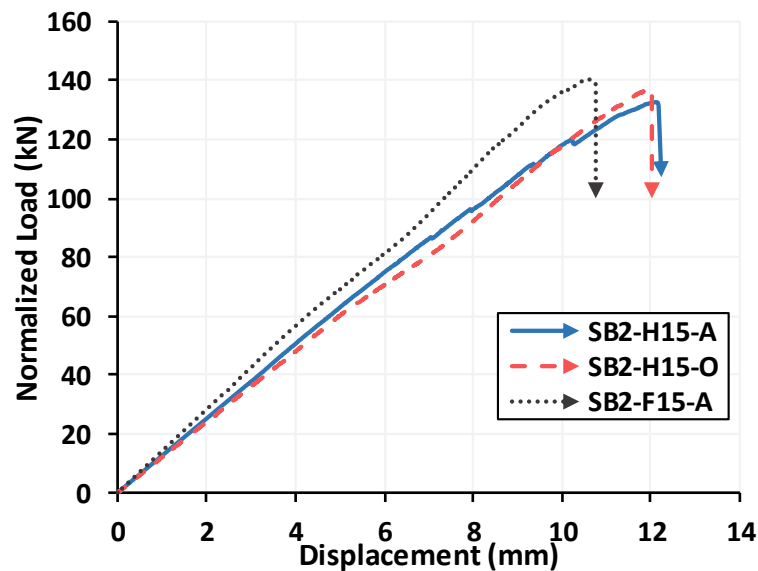


Figure 4.21 Load-deflection curves for specimens SB2-H15-A, SB2-H15-A, and SB2-F15-A

4.3.5. HFRP and CFRP Strains

Figures 4.22a and 4.22b show typical normalized load-strain curves recorded in the confining CFRP and HFRP sheets of the tested specimens; the relationship is found to be bilinear, similar to what was previously observed in the load-deflection response. Before cracking the slab specimen, a very small strain was recorded in the confining sheets (HFRP or CFRP). However, as the applied load was increased, the concrete slab's tensile cracks started to appear, leading to approximately linear behavior in the load-strain response of the sheets until failure of the specimen occurred.

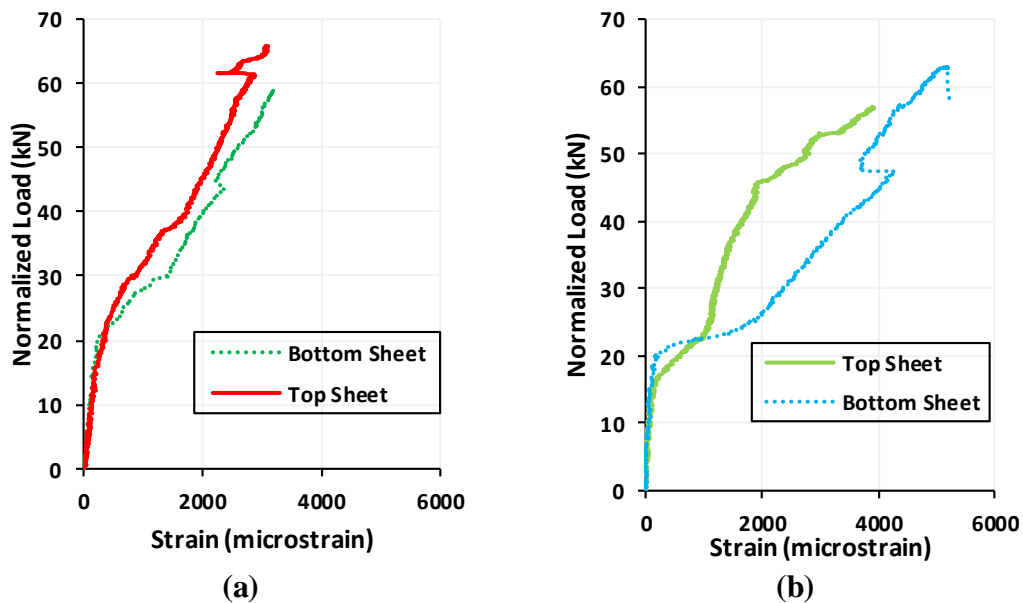


Figure 4.22 Typical load versus strain response for (a) CFRP sheets and (b) HFRP sheets

The maximum strains measured at the center of the HFRP and CFRP confining sheets of all tested specimens are summarized in Table 4.2. The bottom sheets are the ones that were placed first and are directly attached to the concrete surface, and the top sheets are the ones placed in the normal direction above the bottom ones. Generally, the strain is much higher in specimens with a reinforcement ratio of 1% (series SA1 and SB1) than in slabs with a reinforcement ratio of 1.5% (series SA2 and SB2); this can be explained by the fact that the tensile cracks are more likely to appear in reinforced

members with a low reinforcement ratio. Referring to **Table 4.2**, the bottom sheets in series SB1 and SB2 experienced higher strains than the top sheets; this is supposed because the bottom sheets experienced more stress than the top sheet, causing them to be rupture earlier. On the other hand, the offset sheets had higher strains than the adjacent ones in all series; this could be attributed to the fact that the offset sheet covered most of generating major cracks.

Table 4.2 Measured (HFRP-CFRP) ultimate strain

Specimen	Ultimate strain ($\mu\epsilon$)	
	Location of strain gauge	
	Bottom sheets	Top sheets
SA1		
SA1-H10-A	11,057.8	6,619.5
SA1-H10-O	-	-
SA1-H15-A	3,660.8	-
SA1-H15-O	3,928	5,223.4
SA1-H20-A	-	5,773.2
SA1-F15-A	3,219.8	3,105.1
SA2		
SA2-H15-A	3,547.1	1,978.7
SA2-H15-O	6,294.7	7,011.9
SA2-H20-A	11,083.9	4,593.9
SA2-F15-A	3,678.9	6,914.4
SB1		
SB1-H15-A	6,517.5	4,184.2
SB1-H15-O	9,750.8	2,572.5
SB1-H20-A	9,137.4	-
SB1-H15(2)-A	4,226.2	4,858.1
SB1-F15-A	6,767.1	5,223.8
SB2		
SB2-H15-A	4,600.4	4,538.3
SB2-H15-O	4,775.3	4,008.6
SB2-H20-A	4,762	7,742.6
SB2-H15(2)-A	4,829.8	6,903.9
SB2-F15-A	5,230.6	4,116.2

CHAPTER 5

NUMERICAL AND ANALYTICAL INVESTIGATIONS

5.1. Introduction

In this chapter, the experimental results of the interior slab-column connection are validated numerically and analytically. Numerical modeling was performed using the finite element approach with the ABAQUS software, while analytical modeling was conducted by adopting Mowrer and Vanderbilt's equation that determines the punching shear strength of the slab based on its flexural capacity. The following sections present the details of the numerical and analytical procedures.

5.2. Part One: Numerical Modeling

This section presents the numerical procedure for two different models. Model 1 simulates the compression test of a standard 6x12 in. (150x300 mm) concrete cylinder to verify the experimental program's material. Model 2 simulates an interior slab-column connection strengthened by composite materials. The numerical modeling objective is to determine the tested specimens' performance using a numerical approach; the following connections (SB1, SB1-H15-A, and SB1-F15-A) are adopted to achieve this objective.

5.2.1. Finite Element Method

The finite elements method (FEM) is commonly used to model reinforced concrete structures' behavior under applied loads. The FEM allows solving partial

differential equations in two or three variables. FEM can solve the problem by subdividing a large system into smaller parts that are called finite elements.

5.2.2. Concrete Damaged Plasticity (CDP)

5.2.2.1. Literature

A series of researches used Concrete Damaged Plasticity (CDP) to simulate RC connections.

Genikomsou and Polak, (2016) simulated four interior reinforced concrete slab-column connections with shear reinforcement using the ABAQUS package's finite element method. The damaged plasticity model in ABAQUS was adopted to simulate the concrete material properly. The numerical findings were compared to experimental results; they found that the concrete model's calibration is an important step in the FEA. Furthermore, they reported that the FEA's load-deflection responses and cracking propagation of the simulated connections were closely aligned with the experimental results.

Silva et al., (2019) conducted experimental and numerical studies to examine the effect of externally bonded CFRP sheets in the punching shear capacity of interior slab column connections. They used the ABAQUS package to simulate the experimental program that offers concrete damaged plasticity for modeling concrete material. The numerical results showed that the model predicted the connections' behavior in good agreement with the test results.

Hamoda and Hossain, (2019) developed nonlinear three-dimensional finite element (FE) models to evaluate the behavior of two-way reinforced concrete (RC) slab-column connection with additional punching-shear reinforcement. They concluded

that a sensitive study for the main numerical parameters, including the viscosity parameter (μ) and mesh size, is needed to get better numerical results. They further stated that a strong agreement between numerical and experimental results was observed.

5.2.2.2. Concrete Damage Plasticity (CDP)

The behavior of the concrete was studied by Lubliner et al., (1989), who introduced one of the most important models, which adopted later by ABAQUS under the name of concrete damage plasticity (CDP) (**Figure 5.1**); this followed by some modifications by Lee and Fenves, (1998). This model is a continuum, plasticity-based, damaged model for concrete behavior. It is governed by two main failure mechanisms of the concrete material: tensile cracking and compressive crushing.

A full representation of CDP equations can be observed in following steps:

$$Y = \frac{1}{1-\alpha} \left[\sqrt{3J_2} + \alpha I_1 + \beta * \varepsilon^{Pl} \langle \bar{f}_{max} \rangle - \gamma \langle -\bar{f}_{max} \rangle \right] - \bar{f}_{max} * \varepsilon^{Pl} \dots (1)$$

where:

- Y : yield surface.
- $\sqrt{3J_2}$: is the classical deviatoric stress measure.
- I_1 : is the hydrostatic pressure.
- $\langle \bar{f}_{max} \rangle$: the algebraically maximum principal stress.
- α , β and γ are dimensionless constant values.

The parameter α can be obtained by comparing the initial biaxial and uniaxial compressive yield stresses fbo and fco according to Equation 2:

$$\alpha = \frac{\left(\frac{fbo}{fco}\right)^{-1}}{2\left(\frac{fbo}{fco}\right)^{-1} - 1} \dots (2)$$

where $\left(\frac{f_{bo}}{f_{c0}}\right)$ can be ranged between 1.10 and 1.16 (in the current investigations this value was considered as 1.16 due to the acceptable observed results).

The parameter γ can be determined by comparing the yield conditions along the tensile and compressive meridians. This coefficient is obtained according to Equation 3:

$$\gamma = \frac{3(1-Kc)}{2Kc-1} \dots (3)$$

where the ratio Kc ranges between about 0.64 and 0.8. The CDP model assumes a default value of $2/3$ for Kc based on triaxial stress test results.

The dimensionless parameter β is defined as:

$$\beta(\widetilde{\varepsilon}^{Pl}) = \frac{\bar{\sigma}c(\widetilde{\varepsilon}c^{Pl})}{\bar{\sigma}t(\widetilde{\varepsilon}t^{Pl})} (1 - \alpha) - (1 + \alpha) \dots (4)$$

where $\bar{\sigma}c(\widetilde{\varepsilon}c^{Pl})$ and $\bar{\sigma}t(\widetilde{\varepsilon}t^{Pl})$ are effective compressive and tensile cohesion stresses, respectively.

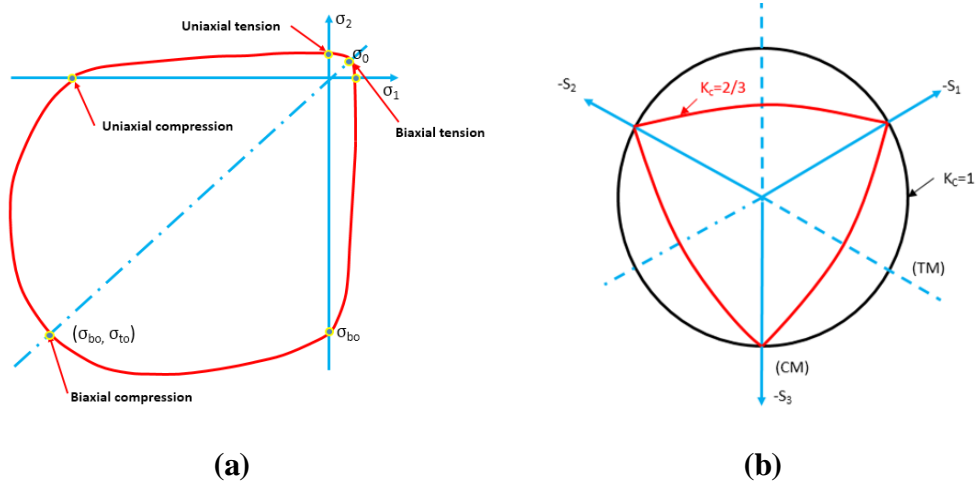


Figure 5.1 The yield surface in: (a) plane stress cross section and (b) deviatory plane; Lubliner et al. (1989)

As illustrated in **Figure 5.2**, the plastic behavior in CDP is represented by the compression and tensile response. The evolution of the damage due to the compression (dc) of the concrete is related to the plastic deformation, which is determined by the inelastic deformation $\varepsilon_c^{in} = \varepsilon_c - \sigma_c Ec^{-1}$ using a constant factor bc equals $0 < bc \leq 1$.

$$dc = 1 - \frac{\sigma_c E^{-1}}{\epsilon_c^{Pl} \left(\frac{1}{b_c} - 1 \right) + \sigma_c E C^{-1}} \quad \dots (5)$$

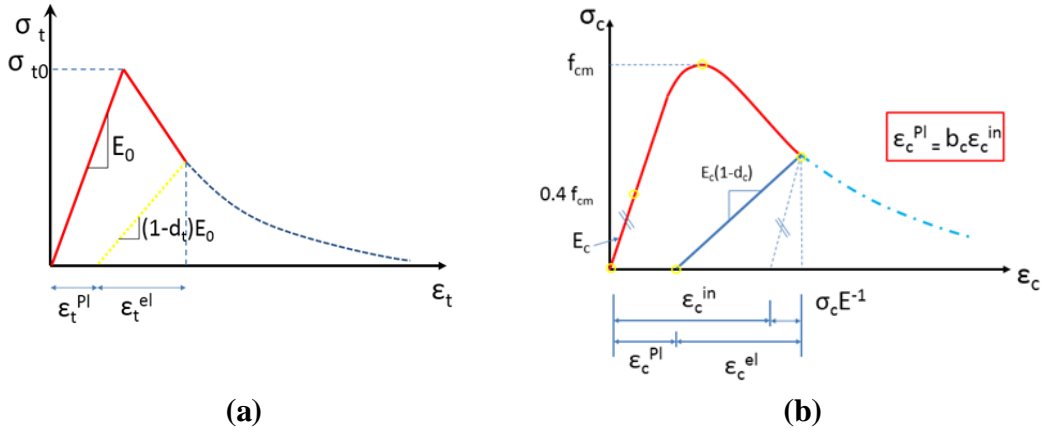


Figure 5.2 Response of concrete to uniaxial loading in (a) tension and (b) compression; (Smith 2009)

Similarly, the damage parameter in tension of the concrete bt depends on the plastic deformation ϵ_c^{Pl} .

The selected CDP parameters adopted in this investigation are listed in **Table 5.1**.

Table 5.1 Concrete parameters

Dilation angle	36
Eccentricity	0.1
Biaxial and uniaxial resistance ratio in compression	$f_{b0}/f_{c0} = 1.16$
KC	0.667

5.2.3. Model 1: Compression Test for Concrete Cylinder (Material Verification)

To capture better numerical results for the tested specimens, the concrete used was verified by Model 1, which simulates the concrete cylinder subjected to compression loading. After that, the numerical stress-strain curve is compared to the experimental curve obtained by testing 150x300 mm standard cylinders according to ASTM C39, (2010).

5.2.3.1. Laboratory Test

Three standard concrete cylinders ($\varnothing = 150 \text{ mm}, l = 300 \text{ mm}$) were cast from different batches. The cylinder specimens were left in the curing room for 28 days. The compression test was conducted considering the requirements of the ASTM C39 standard. The tested cylinders were subjected to a static monotonic loading with a 1 mm/min rate until failure using Tinius Olsen Testing Machine. Four LVDT's were located on the specimen's lateral surface to get the vertical displacement and were parallel to the vertical axis. The test setup is shown **Figure 5.3**.

The average values of load-displacement responses obtained from the laboratory test were used to determine the concrete's stress-strain relationship (**Figure 4.4**). The experimental properties of the concrete used in this study are listed in **Table 5.2**.

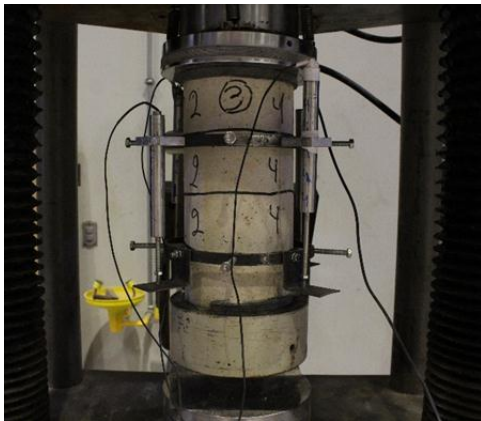


Figure 5.3 The concrete sample subjected to compression test

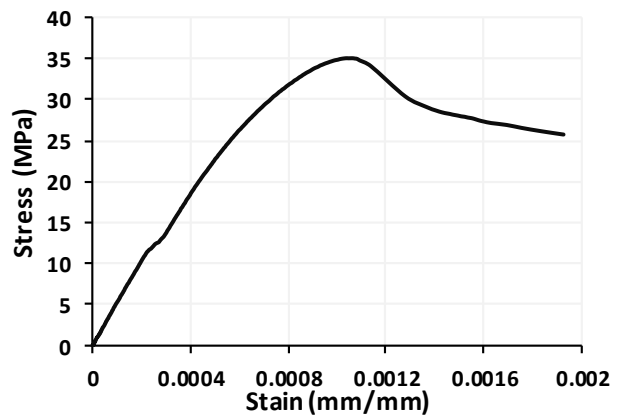


Figure 5.4 Stress-strain relationship for the concrete

Table 5.2 Concrete properties

Concrete	Compressive strength (MPa)	Modulus of elasticity (MPa)	Strain at Ultimate Stress
	35	45000	0.001065

5.2.3.2. Finite Element Model

5.2.3.2.1. Model Geometry and Boundary Conditions

A nonlinear 3D FEM model was prepared in the ABAQUS program to simulate the concrete cylinder under a compression test. The model consisted of a 150x300 mm cylinder modeled as a solid part simulated with an eight-node brick element with reduced integration (C3D8R) by performing displacement control analysis in ABAQUS/Standard. The model is portioned in a way that allows having a uniform mesh (**Figure 5.5**). The CDP approach was adopted to model the concrete material; all parameters are considered based on the previously presented information in Section 5.2.2.2 (**Figure 5.2**). To attach the boundary conditions, vertical rollers ($U_2 = 0$) were assigned on the bottom surface of the cylinder; in order to create a stable structure system, a pin ($U_1 = U_2 = U_3 = 0$) was assigned at a node located on the center of the bottom surface of the cylinder (**Figure 5.6**). The stress-strain diagram was recorded at a reference point associated with the upper surface of the cylinder.

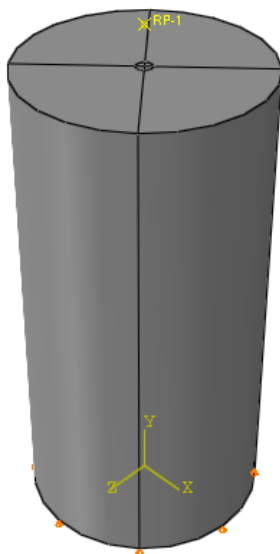


Figure 5.5 3D representation of the model

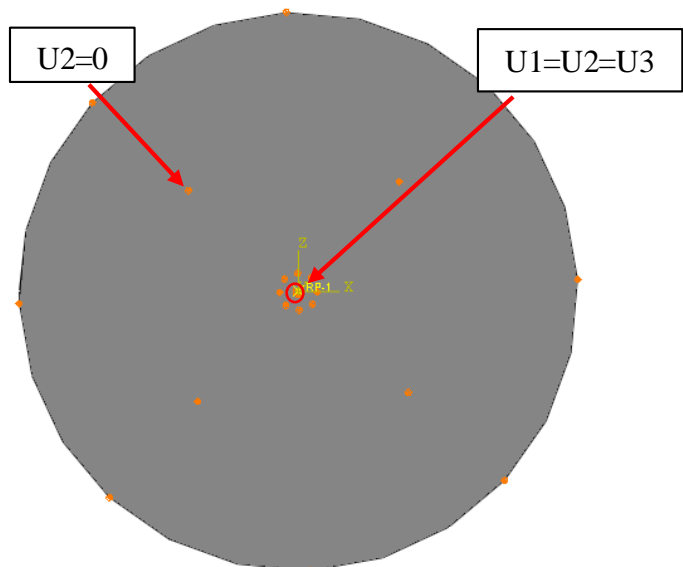


Figure 5.6 Boundary conditions used in the numerical model

5.2.3.2.2. Calibration of the Model

- Mesh

Mesh sensitivity analysis was performed with different mesh sizes ranging from 15 to 2.5 mm to obtain the best results in terms of ultimate stress. The finite element results against different mesh sizes are presented in **Figure 5.7**. It is notable that when the coarse mesh (15 mm) is used, a slight difference is observed in the ultimate stress relative to the experimental result. This difference decreases as the mesh size decreases. It should be mentioned that mesh sizes 5 and 2.5 mm provide the most accurate results, as the relative errors between numerical and experimental results in these cases are 1.43% and 0.43%, respectively. However, to reduce the computational expenses (**Table 5.3**), the viscosity parameter is calibrated at a mesh size equal to 5 mm in the next section.

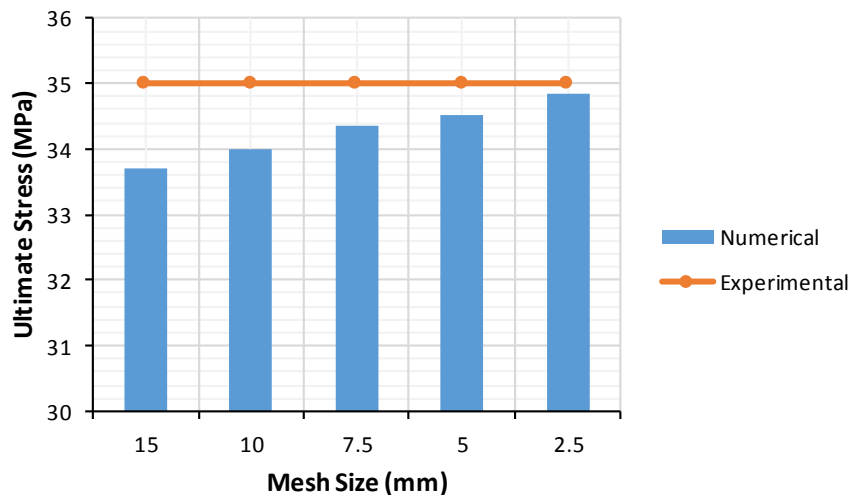


Figure 5.7 Experimental vs. Numerical results for different mesh sizes

Table 5.3 Mesh sizes and No. of elements for the concrete cylinder

No.	Mesh Size (mm)	No. of Elements
1	15	1920
2	10	5760
3	7.5	12800
4	5	43200
5	2.5	379200

- Viscosity Parameter

The viscosity parameter is one of the most important properties of the CDP model that introducing rate dependence into the material as relaxation time. A parametric study was performed to investigate the sensitivity of viscosity parameter on numerical simulation of the concrete cylinder. Four values for the viscosity parameter were considered: $\mu = 0.01, 0.001, 0.0001, \text{ and } 0.00001$. **Figure 5.8** presents the comparison between the numerical and experimental stress-strain curves. It is shown that the optimum value of the parameter can be taken as 0.0001, giving a very accurate numerical result in terms of stress-strain response for the concrete used. It is worth mentioning that viscosity= 0.00001 also provided an accurate result. However, it increases the duration of the analysis. Thus, the viscosity parameter 0.0001, found through this numerical investigation, is considered the most appropriate to simulate the subsequent slab-column connections.

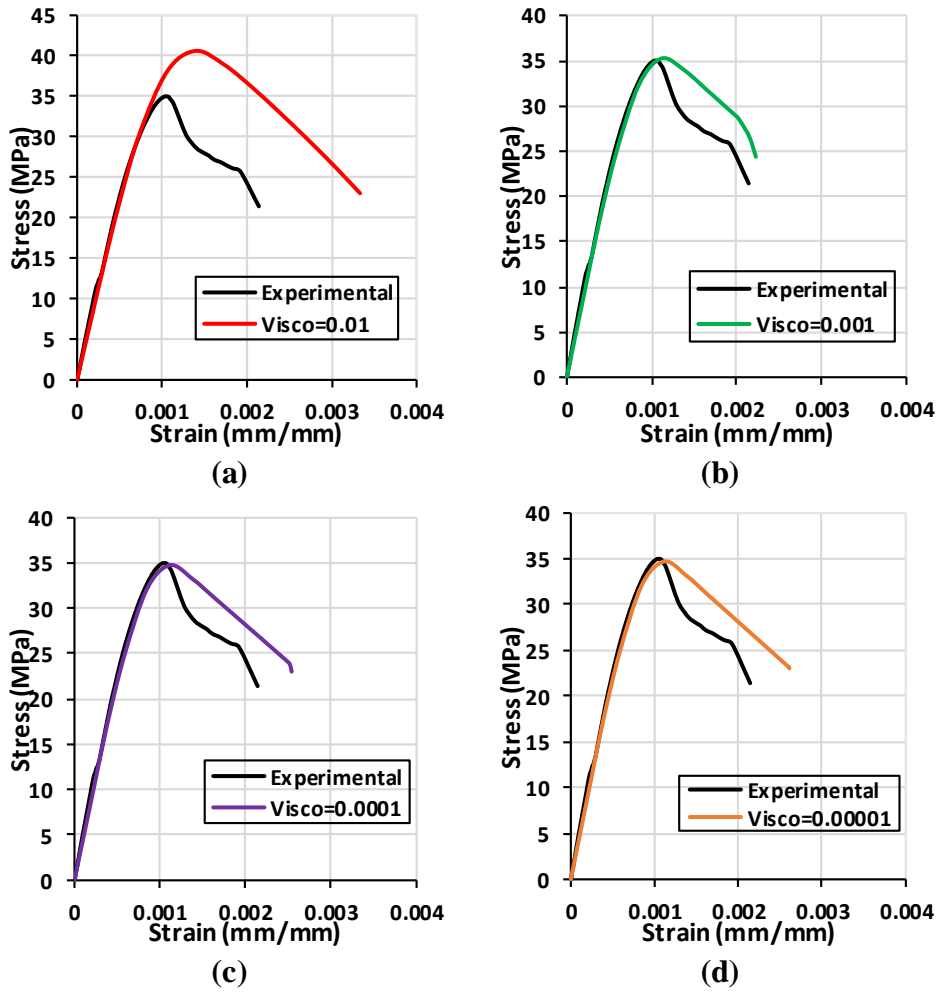


Figure 5.8 Stress-strain curves using different values of viscosity parameter

5.2.4. Model 2: Slab-Column Connection

After the numerical investigation and verification of the concrete material used in the experimental program in the previous section; herein, a nonlinear 3D FEM model was used to simulate interior slab-column connection strengthened by composite materials. Three connections are analyzed in terms of load-displacement response. SB1 represents control specimens, SB1-H15-A represents connections strengthened by HFRP, and SB1-F15-A represents connections strengthened by CFRP.

5.2.4.1. Finite Element Model

5.2.4.1.1. Model Construction

Model 2 consists of four main parts: slab, reinforcement steel, strengthening sheets, and support system. The slab was considered a deformable solid part simulated with an eight-node brick element with reduced integration (C3D8R). However, the reinforcement steel was modeled as a wire deformable element 2-node linear 2-D truss (T3D2) embedded in the concrete element assuming a perfect bond between two materials (Silva et al., 2019). A mesh size of 5 mm was introduced for the steel bars. The strengthening sheets were modeled using a 4-node doubly curved shell element (SAR) with mesh size equal to 10 mm and bonded to the concrete surface by cohesive interaction. The adhesive material properties used to assign the cohesive interaction are listed in **Table 5.4**. A rigid body constraint was assigned to the support system to reduce computational time and neglect its stress. The interaction between the support and concrete is normal hard contact and tangential contact with a 0.2 friction coefficient.

Table 5.4 Material properties of adhesive

Parameters	Sikadur 330 (Kabir et al. 2016)
E_a (GPa)	4.82
t_n (MPa)	31.28
t_s (MPa)	31.28
t_t (MPa)	31.28
K_{nn} (N/mm ³)	4.72×10^{13}
K_{ss} (N/mm ³)	2.36×10^{13}
K_{tt} (N/mm ³)	2.36×10^{13}
G_n (N/mm)	1
G_s (N/mm)	1.25
G_t (N/mm)	1.25

Due to the specimens' symmetry, only one-quarter of the specimen was modeled with relevant boundary conditions to reduce the analysis's computational time. The

boundary conditions consisted of a fixed constrain, which was assigned on the reference point of the rigid support, and the symmetric planes were restrained in their perpendicular directions, as shown in **Figure 5.9**. The connection was subjected to load through a rigid pad placed above the column stub with displacement control in ABAQUS/Standard.

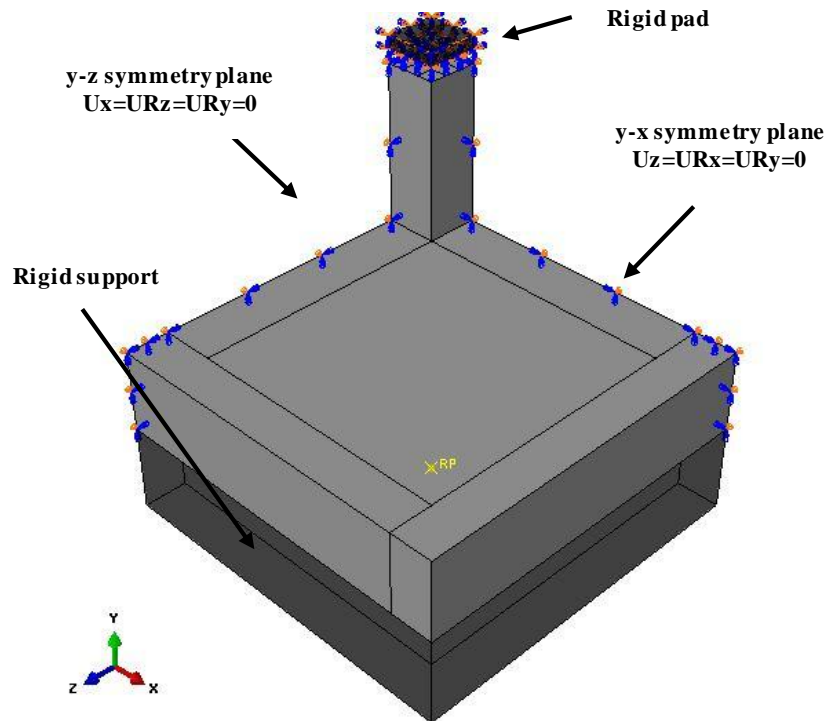


Figure 5.9 Geometry and boundary conditions of Model 2

5.2.4.1.3. Materials

Concrete material properties are the same as the first validated Model 1 and are listed in **Table 5.5**. The steel's behavior in the numerical model was introduced as elastic-plastic material; the reinforced steel bars properties are presented in **Table 5.6**. The behavior of the composite sheets was modeled as elastic lamina with fail stress. In general, two types of composites were used to reinforce the connection: HFRP and CFRP. The mechanical properties used in the numerical model are shown in **Table 5.7**.

Table 5.5 Damage properties of concrete

Dilation Angle	Eccentricity	F_{b0}/f_{c0}	Kc	Viscosity Parameter
36	0.1	1.16	0.667	0.0001

Table 5.6 Steel reinforcement properties for Model 2

Parameter	value
Modulus of elasticity (MPa)	210,000
Poison's ratio	0.3
Yield stress (MPa)	570
Failure stress (MPa)	640

Table 5.7 Composite material properties for Model 2

Parameter	CFRP	HFRP
Tensile strength (MPa)	3500	30
Modulus of elasticity (MPa)	230,000	3700
Poison's ratio	0.25	0.3
Thickness (mm)	0.13	1.2

5.2.4.1.4. Calibration of the Model

- Mesh

A mesh sensitivity analysis was conducted to determine the best mesh size that provides the most comparable results in term of ultimate load. Three mesh sizes (15 mm, 20 mm, and 25 mm) are adopted in this investigation. These selected values should be larger than the aggregate size (10 mm) but not too large leading to a coarse mesh (A. Genikomsou 2018). The mesh size 15 mm divided the slab thickness into five elements, while the mesh sizes of 20 and 25 mm, divided it into 4 and 3 elements. **Figure 5.10** presents the results of ultimate load against different mesh sizes. The results are mesh-dependent, where the coarse (25 mm) and the fine (15 mm) mesh sizes provide load values away from the experimental results. However, mesh size 20 mm showed an excellent agreement with the test data, as already observed in other studies (A.

Genikomsou 2018; Hamoda and Hossain 2019). This mesh size (20 mm) is considered in all subsequent simulations.

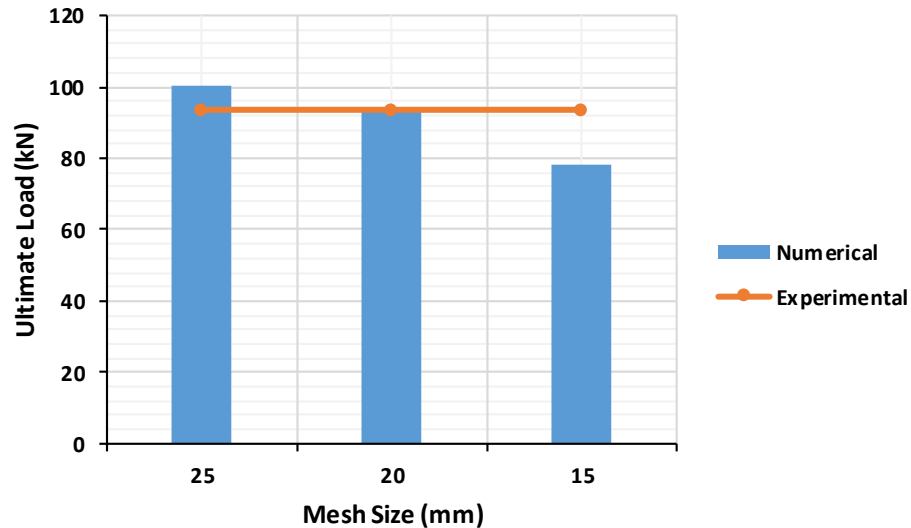


Figure 5.10 Experimental vs. Numerical results for different mesh sizes

- Springs

During the laboratory test, a steel cap with rubber was used on the top of the column stub to ensure the column would not fail before the slab. However, due to the fact the LVDT's were placed above this cap, the load-displacement reading is highly affected by the existence of rubber material. In order to consider the effect of the rubber pad on the load-displacement response, a square rigid part with dimensions 50x50x12.7 mm was introduced to the model and then connected to the top of the column stub by 16 springs (4x4) with an initial length $L_o = 12.7$ mm spaced at 12.5 mm (**Figure 5.11**). The current FE model was re-executed several trials to capture the most suitable stiffness property (K) of the springs. **Figure 5.12** shows the load-deflection curve for some of these trials. The load-deflection response of the model with a $K=190$ N/mm showed a good agreement with that of the experimental one compared to other stiffnesses.

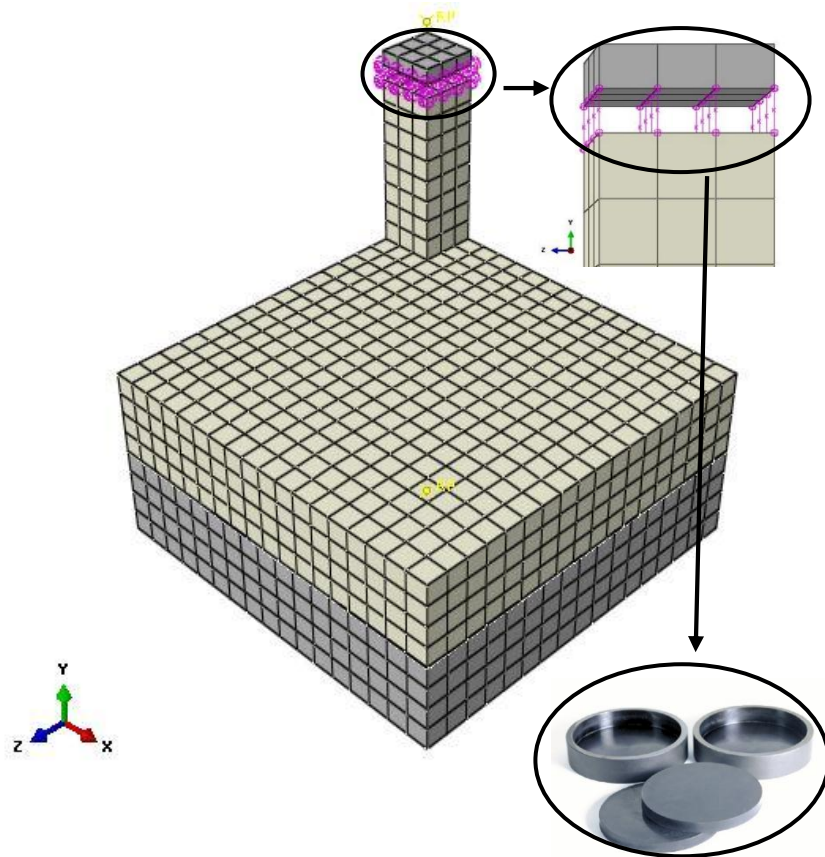


Figure 5.11 Mesh scheme and springs representation

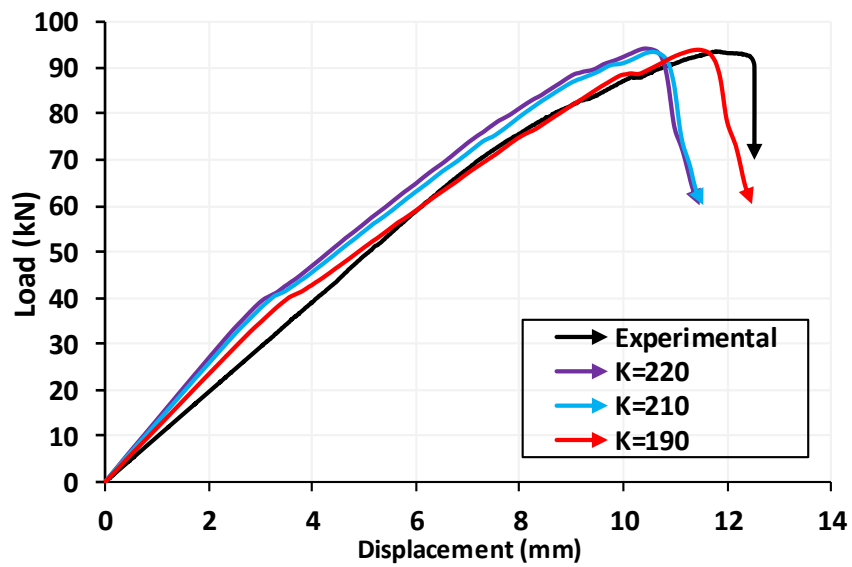


Figure 5.12 Load-displacement response for the numerical model with different values of (K)

5.2.4.2. Finite Element Results and Discussion

The numerical results are studied by comparing the simulated connection's behavior with the experimental results in terms of cracking pattern, load-deflection response, ultimate load, and ultimate displacement. **Figure 5.13** displays the deflection of the connection provided by numerical analysis. The maximum deflection is detected at the center of the connection. A slight uplift of corners was noted during testing; the numerical model validated this observation. A positive contours color was observed at the edges of the connection representing the corners' uplifting.

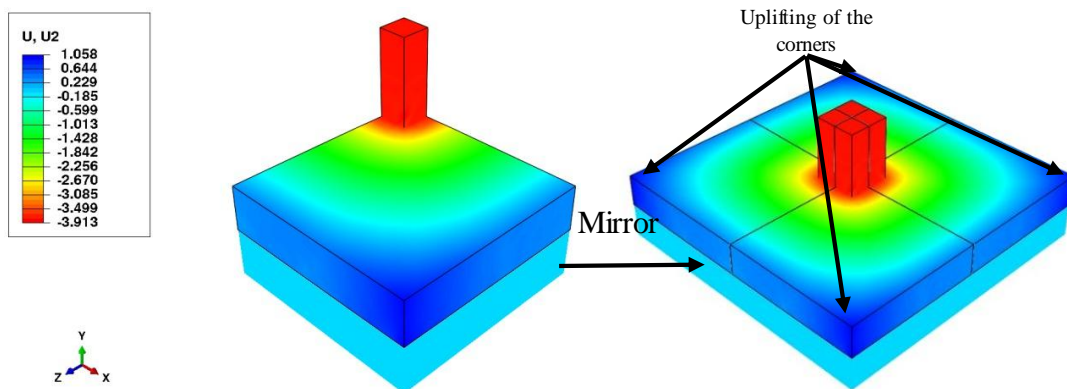
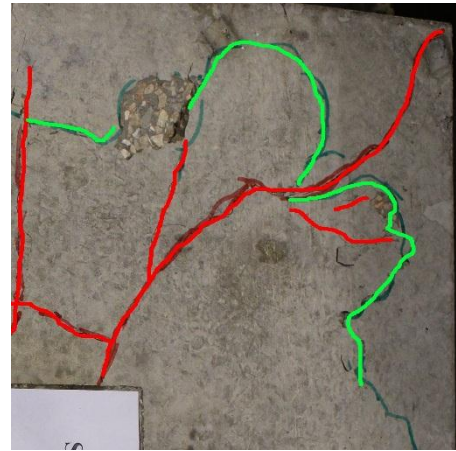
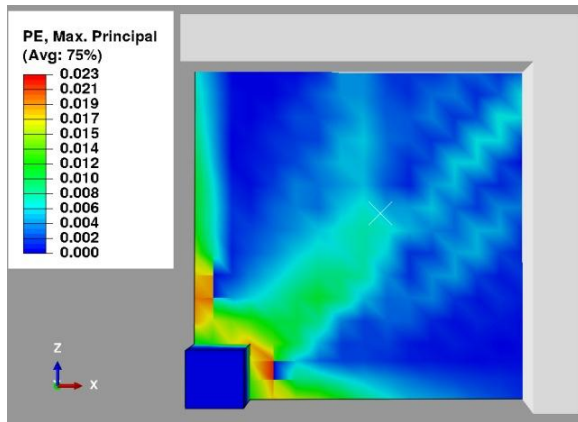
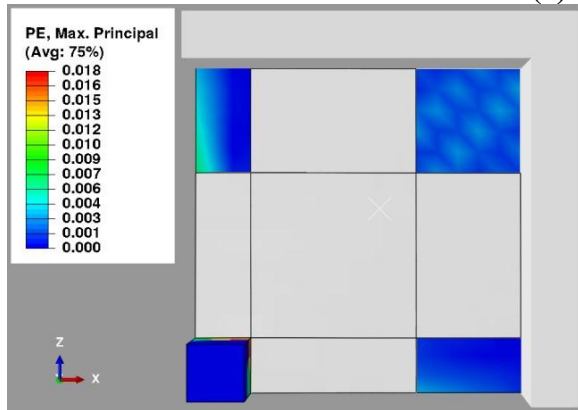


Figure 5.13 Deflection shape at failure load

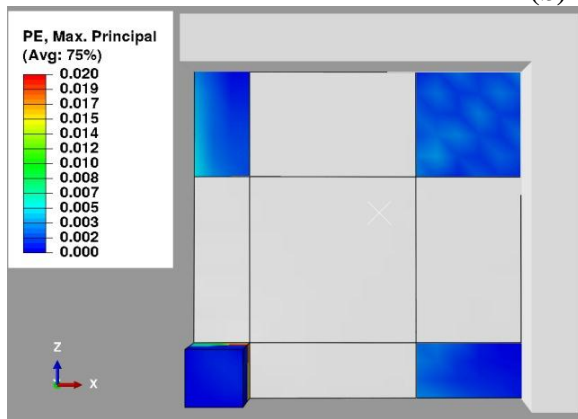
In the numerical analysis, plastic strain (PE) was used to present the connections' cracking pattern. **Figure 5.14** compares the experimental and numerical crack pattern on the simulated connections' tension surface at ultimate failure load. The plastic strain contour and the experimental propagated cracks are approximately the same in the simulated connections. Therefore, the FE model can predict the development of the cracks of slab-column connection.



(a)



(b)



(c)

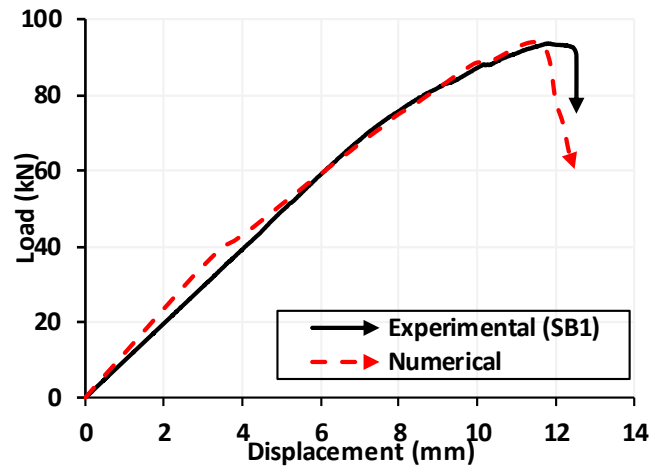
Figure 5.14 Comparison of crack patterns (a) SB1; (b) SB1-H15-A; and (c) SB1-F15-A

A comparison between the experimental and numerical results is presented in **Table 5.8**. The numerical model provided a very similar ultimate load to the experimental results, where the relative errors between numerical and experimental results for specimens SB1, SB1-H15-A, and SB1-F15-A are 0.385%, 0.4%, and 3.945%, respectively. The numerical values for the displacement of SB1, SB1-H15-A, and SB1-F15-A, at ultimate load, are 11.445, 11.226, and 12.235 mm, respectively, comparable to the experimental results (11.77, 10.093, and 11 mm, respectively).

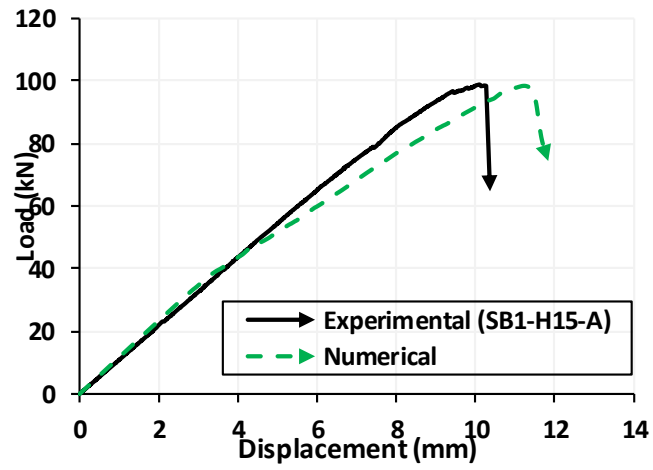
Figure 5.15 compares the numerical and experimental load-deflection response for the simulated specimens. It clearly shows that the numerical model can predict the mode of failure of the specimen, where pure punching shear failure is observed (which is characterized by a sharp drop in load) in numerical curves as happened in the experimental. For the un-strengthened specimen (SB1), the numerical model provides a strong alignment in load-deflection response with experimental results. However, the numerical load-deflection curve's initial stiffness for strengthened specimens (SB1-H15-A and SB1-F15-A) is matched with the experimental curve; then, the FE model provided lower stiffness than the experimental one.

Table 5.8 Comparison between experimental and numerical results

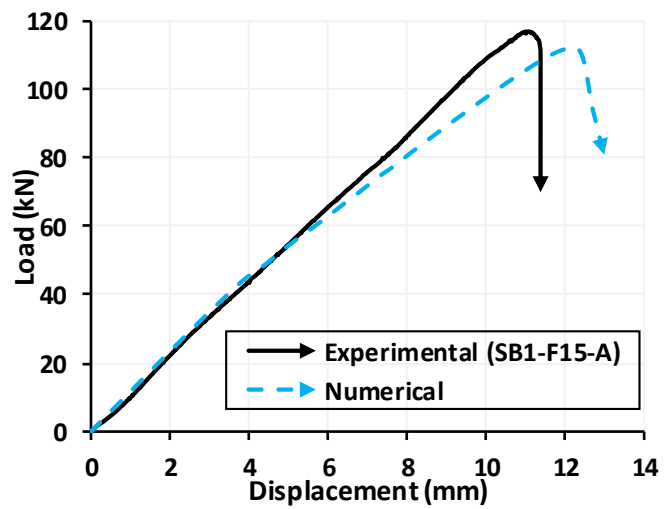
Specimen	Experimental Results		Numerical Results	
	Ultimate Load (PU _{exp}) (kN)	Deflection at PU (Δ _{exp}) (mm)	Ultimate Load (PU _{FEM}) (kN)	Deflection at PU (Δ _{FEM}) (mm)
SB1	93.57	11.77	93.93	11.445
SB1-H15-A	98.9	10.093	98.5	11.226
SB1-F15-A	117.0166	11	112.4	12.235



(a)



(b)



(c)

Figure 5.15 Load-deflection responses (a) SB1; (b) SB1-H15-A; and (c) SB1-F15-A

5.3. Part Two: Analytical Modeling

This section presents the analytical model procedure used to calculate the punching shear capacity for both un-strengthened and strengthened specimens. A comparison between the analytical values, the experimental results, and the values calculated using the ACI Building Code equation (ACI 318-08 2008) will be presented.

5.3.1. Analytical Model

The equation proposed by Mowrer and Vanderbilt, (1967) was selected to predict the two-way shear strength of the connections. They suggested that the punching shear capacity of the slab can be determined based on its flexural strength:

$$P_u = \frac{0.8(1+d/r)bd\sqrt{f'_c}}{1 + \left(0.433bd\frac{\sqrt{f'_c}}{P_{flex}}\right)} \dots (7)$$

where:

- P_u : two-way shear strength.
- $\sqrt{f'_c}$: compressive strength of the concrete (MPa).
- d : depth of internal ordinary tension reinforcement.
- r : width of the column.
- b : perimeter of column.
- P_{flex} : load applied to cause flexural yielding.

The term P_{flex} can be calculated based on the formation of a yield line analysis of a slab at ultimate strength.

$$P_{flex} = 8m \left(\frac{1}{1-r/w} - 3 + 2\sqrt{2} \right) \dots (8)$$

where:

- w : width of the slab.
- m : flexural capacity of the specimen.

The specimen's flexural capacity was computed by performing a cross-section analysis based on force equilibrium and strain compatibility, considering the effect of concrete, steel reinforcement, and composite materials. The following assumptions were considered during the analysis:

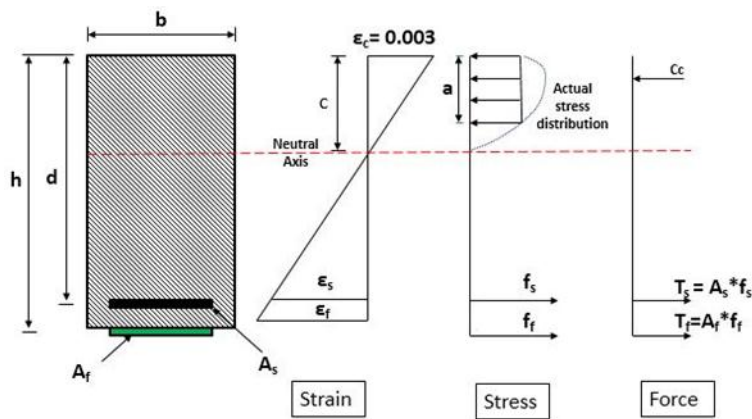


Figure 5.16 Strain, stress, and force distribution in section

- Strain in the concrete and the reinforcement are directly proportional to the distance from the neutral axis.
- The maximum ultimate strain at the extreme concrete compression fiber is assumed to equal 0.003.
- There is a perfect bond between the hemp composite and the concrete surface.

The neutral axis depth c can be obtained iteratively from the equilibrium of forces until the following equation is satisfied

$$C_c = T_s + T_f \dots (9)$$

where:

- T_s : tensile force of the reinforcement bars.
- T_f : tensile force of the composite sheets

The area of the composite sheets including the effects of strengthening configuration can be calculated by the model proposed by Sharaf et al., (2006):

$$A_f = \sum_{i=1}^n \frac{\eta}{\zeta} b_{fi} t_{fi} \dots (10)$$

where:

- b_{fi} : width of composite sheet.
- t_{fi} : thickness of composite sheet.
- η : factor that represents the effect of composite sheets orientation [1 for orthogonal sheets]
- ζ : factor that accounts for the effect of composite sheets location relative to the column face. Can be calculated as follows:

$$\zeta = \frac{\sum_{i=1}^n \frac{b_{fi}}{s_i}}{n} \dots (11)$$

- s_i : the distance from center of each composite sheet to the column face.
- n : the total number of composite sheets per slab width.

Finally, the flexural strength can be determined as follows:

$$M_n = T_s \left(d - \frac{a}{2} \right) + T_f \left(h - \frac{a}{2} \right) \dots (12)$$

where:

- h : slab thickness.
- a : depth of the rectangular concrete stress block.

Furthermore, considering the contribution of the composite material, the equivalent depth of the slab d_{eqv} can be backwardly determined by:

$$d_{eqv} = \frac{M_n}{T_s + T_f} + \frac{a}{2} \dots (13)$$

The punching shear capacity for slab strengthened by composite material can be predicted by replacing d by d_{eqv} in equation (7).

5.3.2. American Concrete Institute (ACI) Building Code

The experimental results are also compared to the ACI code equation (ACI 318-08 2008). ACI code suggests that the major variables that affect the slab's punching shear capacity are concrete compressive strength, development length, and the column dimension. However, the ACI neglects the effect of the steel reinforcement ratio. The ACI equation for the two-way shear strength is:

$$P_u = \left(0.17 + \frac{0.33}{\beta_c}\right) \sqrt{f'_c} b_o d \leq 0.33 \lambda \phi_c \sqrt{f'_c} b_o d \dots (14)$$

where:

- λ : factor used to account for low density concrete [1 for normal density concrete]
- ϕ_c : strength reduction factor for concrete [assumed 1 for this investigation]
- β_c : ratio of the long side to the short side of the column.
- b_o : the perimeter of the critical section for punching shear taken at a distance of $\frac{d}{2}$ from the face of the column.

5.3.3. Analytical Results and Discussion

Table 5.9 summarizes the comparison between the analytical and ACI Code results relative to the experimental results. It can be noted that the analytical model proposed by Mowrer and Vanderbilt (1967) provides a good prediction of the punching shear capacity for the tested specimens. The average ratio of the experimental punching shear strength values to the analytical predictions $P_{u\text{ test}}/P_{u\text{ calc}}$ is 1.044 with a standard deviation of 0.113. On the other hand, the ACI Code provides a very conservative prediction for the punching shear capacity. The average ratio $P_{u\text{ test}}/P_{u\text{ calc}}$ is 1.7 with a standard deviation of 0.27 using the ACI equation. The under-estimation of the ACI Code for the punching shear capacity of the slab is attributed to the fact that ACI Code (Equation 14) neglects the contribution of flexural reinforcement and does not consider the increase in punching shear strength due to confinement by CFRP or HFRP sheets. If the effective depth d in Equation 14 is replaced by the equivalent effective depth d_{eqv} from Equation 13 (which takes into consideration the effect of confinement), the average ratio $P_{u\text{ test}}/P_{u\text{ calc}}$ using the “Modified” ACI Equation would decrease from 1.7 to 1.59 (**Table 5.9**), which still shows under-estimation of the ACI Equation due to neglecting the contribution of the flexural reinforcement.

Table 5.9 Comparison between experimental and analytical results

Slab specimen	Pu _{test} (kN)	d _{eqv} (mm)	Analytical model		ACI 318-08		Mod ACI 318-08	
			Pu _{calc}	Pu _{test} /Pu _{calc}	Pu _{calc}	Pu _{test} /Pu _{calc}	Pu _{calc}	Pu _{test} /Pu _{calc}
SA1	49	37	48.33	1.014	39.59	1.24	39.59	1.24
SA1-H10-A	45.26	38.76	54.01	0.838	39.59	1.14	42	1.08
SA1-H10-O	53.27	40.35	59.72	0.892	39.59	1.35	44.22	1.20
SA1-H15-A	59.6	39.52	56.66	1.052	39.59	1.51	43.06	1.38
SA1-H15-O	62.935	40.97	62.11	1.013	39.59	1.59	45.1	1.40
SA1-H20-A	69.16	40.2	59.18	1.169	39.59	1.75	44.01	1.57
SA1-F15-A	69.7	42.75	69.54	1.002	39.59	1.76	47.67	1.46
SA2	70.28	37	55.28	1.271	39.59	1.78	39.59	1.78
SA2-H15-A	69.54	38.87	61.78	1.126	39.59	1.76	42.15	1.65
SA2-H15-O	78.715	40.03	66.11	1.191	39.59	1.99	43.77	1.80
SA2-H20-A	74.17	39.41	63.78	1.163	39.59	1.87	42.91	1.73
SA2-F15-A	79.02	41.14	72.15	1.095	39.59	2.00	45.34	1.74
SB1	93.57	55	98.47	0.950	66.57	1.41	66.57	1.41
SB1-H15-A	98.9	56.9	107.24	0.922	66.57	1.49	69.72	1.42
SB1-H15-O	108.25	58.61	115.79	0.935	66.57	1.63	72.6	1.49
SB1-H15(2)-A	102.43	58.47	115.06	0.890	66.57	1.54	72.36	1.42
SB1-H20-A	100.35	57.45	109.94	0.913	66.57	1.51	70.64	1.42
SB1-F15-A	117.01	59.65	121.31	0.965	66.57	1.76	74.37	1.57
SB2	117.26	55	109.21	1.074	66.57	1.76	66.57	1.76
SB2-H15-A	132.65	56.4	115.73	1.146	66.57	1.99	68.88	1.93
SB2-H15-O	136.89	57.72	122.25	1.120	66.57	2.06	71.1	1.93
SB2-H15(2)-A	129.56	57.6	121.69	1.065	66.57	1.95	70.9	1.83
SB2-H20-A	133.9	56.81	117.78	1.137	66.57	2.01	69.56	1.92
SB2-F15-A	140.42	58.55	126.54	1.110	66.57	2.11	72.5	1.94
Average				1.044		1.7		1.59
Standard deviation				0.113		0.27		0.25
Coefficient of variation(%)				10.84		15.9		15.7

CHAPTER 6

CONCLUSIONS AND RECOMMENDATIONS

6.1. Conclusions

This research examines the feasibility of using externally bonded HFRP fabric sheets as punching shear strengthening of reinforced concrete slab-column connections. Twenty-four small-scale interior reinforced concrete slab-column connections were tested in four series: SA1, SA2, SB1, and SB2. SA1 and SA2 included 55 cm thick specimens with 1% and 1.5% reinforcement ratios, respectively. Specimens in series SB1 and SB2 were similar to SA1 and SA2 but had a thickness of 75 cm. The test specimen was subjected to monotonic loading using an MTS machine. The experimental results were following validated through numerical and analytical approaches.

The research focuses on six main parameters that may affect the behavior of strengthened slab-column connections. These parameters are slab thickness, reinforcement steel ratio, HFRP sheet width, location of HFRP sheet relative to the column face, number of HFRP sheets' layers, and confinement type (CFRP or HFRP).

Based on the experimental results, the observations and conclusions can be drawn:

1. Only five specimens experienced combined punching-flexural failure, the remaining specimens failed in pure punching shear failure. The average distance from the face of the column to the punching shear failure plane on the tension face of the specimen was $2.9h$ to $3.8h$ in series SA1 and SA2,

and between 2h to 3.2h for specimens in series SB1 and SB2, with no significant change introduced as a result of strengthening sheets (h is the slab thickness).

2. The tested connections' overall response was almost bilinear up to the ultimate load and can be divided into two phases. The first phase is characterized by the initial stiffness of the un-cracked slab. The second phase can be identified by stiffness reduction due to the development of tensile cracks. After the ultimate load, specimens that experienced pure punching shear failure had a very sharp drop in load whereas specimens that had combined punching-flexural failure experienced relatively more considerable deflections before the occurrence of a sharp drop of the load.
3. Increasing the slab thickness from 55 to 75 mm led to a significant increase in the load-deflection curves' initial stiffness and the ultimate load capacity. The increase in shear capacity reached 90.9% and 66.8% for specimens with 1% and 1.5% reinforcement ratios, respectively. The same conclusion can be drawn for increasing the flexural reinforcement ratio from 1% to 1.5%. The enhancement in shear capacity reached 43.4% and 25.3% for slabs with 55 mm and 75 mm thicknesses, respectively.
4. The test results demonstrated that interior slab-column connections' structural behavior was considerably improved using externally bonded HFRP sheets based on the slab thickness, steel content, width, and configuration for HFRP sheets. The improvement in the ultimate shear capacity ranged between 5.5% and 41.14%, while the increase in stiffness reached up to 56.8% relative to the control specimen.

5. In general, HFRP sheets placed at $1.5d$ offset from the column face, produced a relatively higher increase in the shear capacity of the interior slab-column connections than the HFRP sheets placed adjacent to the column face (d is the effective depth to the reinforcing bars).
6. Adding more layers of hemp fiber fabric composite does not improve the structural behavior of interior slab-column connections due to the premature rupture failure of the second HFRP sheet. This means that specimens strengthened with double HFRP layers exhibit almost the same performance as specimens strengthened with a single layer.
7. Although the performance of specimens strengthened by synthetic CFRP sheets was superior as compared to the natural HFRP confined specimen due to the big difference in the two materials' mechanical properties, this improved performance could be reached by the natural HFRP sheets when they were applied in larger width or different configurations (HFRP sheets with offset from the column).
8. A numerical model was prepared using the finite element method to predict tested specimens' performance. The numerical model accuracy was validated against three tested specimens SB1, SB1-H15-A, and SB1-F15-A. The numerical predictions showed good agreement with experimental results in terms of cracking pattern, load-deflection response, ultimate load, and ultimate displacement.
9. The analytical investigation was conducted by adopting a model proposed by Mowrer and Vanderbilt (1967) to predict the punching shear capacity for strengthened specimens. Comparing the model prediction with the

experimental results showed that the available model provides accurate predictions for the tested specimens' punching capacity. However, the ACI Code gives very conservative predictions in comparison with experimental results.

6.2. Recommendations

Replacing synthetic fibers with natural fibers is a way to achieve sustainable construction. The results of the current investigation concerning using natural hemp fiber fabric sheets as strengthening construction material are promising. However, more research should be done to figure out the best scenario of using externally bonded HFRP sheets. Further research is recommended to:

1. Use eco-friendly adhesive instead of synthetic epoxy resin (Sikadur 330) to bond the HFRP sheets on the concrete surface to reach a higher sustainability level.
2. Investigate the long-term performance of the HFRP-epoxy layer on the structural system.
3. Investigate the behavior of interior slab-column connections strengthened by HFRP sheets under seismic conditions.
4. Investigate the best configuration for applying the HFRP sheets. The skew orientation away from the column face as proposed by Soudki et al. (2011) for CFRP sheets, should be investigated.
5. Investigate new possible techniques to increase the punching shear capacity of strengthened specimens by HFRP sheets, such as using combination of HFRP and steel bolts or using combination HFRP and steel plates.

REFERENCES

- ACI 318-08, ACI. 2008. BUILDING CODE REQUIREMENTS FOR STRUCTURAL CONCRETE (ACI 318-08) AND COMMENTARY. American Concrete Institute, Farmington Hills, Mich. Vol. 2007.
- ASTM C39. 2010. “Standard Test Method for Compressive Strength of Cylindrical Concrete Specimens 1 This Standard Is for EDUCATIONAL USE ONLY.” Annual Book of ASTM Standards, no. C: 1–7. <https://doi.org/10.1520/C0039>.
- ASTM C494. 2015. “Standard Specification for Chemical Admixtures for Concrete.” ASTM International, no. February: 1–10. <https://doi.org/10.1520/C0494>.
- Bitar, Reem, George Saad, Elie Awwad, Helmi El Khatib, and Mounir Mabsout. 2020. “Strengthening Unreinforced Masonry Walls Using Natural Hemp Fibers.” Journal of Building Engineering 30 (February): 101253. <https://doi.org/10.1016/j.jobe.2020.101253>.
- Bourmaud, Alain, and Christophe Baley. 2009. “Rigidity Analysis of Polypropylene/Vegetal Fibre Composites after Recycling.” Polymer Degradation and Stability 94 (3): 297–305. <https://doi.org/10.1016/j.polydegradstab.2008.12.010>.
- Chen, Cheng Chih, and Shun Long Chen. 2020. “Strengthening of Reinforced Concrete Slab-Column Connections with Carbon Fiber Reinforced Polymer Laminates.” Applied Sciences (Switzerland) 10 (1). <https://doi.org/10.3390/app10010265>.
- Chen, Cheng Chih, Chung Yan Li, M. Reza Esfahani, Vahid Moradi, Himat Solanki, and Chandra Khoe. 2006. “Punching Shear Strength of Reinforced Concrete Slabs Strengthened with Glass Fiber-Reinforced Polymer Laminates.” ACI Structural Journal 103 (3): 467–69.

- D3822/D3822M-14, ASTM. 2020. "Standard Test Method for Tensile Properties of Single Textile Fibres" 14 (Reapproved 2020): 1–11. <https://doi.org/10.1520/D3822>.
- Duval, Antoine, Alain Bourmaud, Laurent Augier, and Christophe Baley. 2011. "Influence of the Sampling Area of the Stem on the Mechanical Properties of Hemp Fibers." *Materials Letters* 65 (4): 797–800. <https://doi.org/10.1016/j.matlet.2010.11.053>.
- Eichhorn, S. J., and R. J. Young. 2004. "Composite Micromechanics of Hemp Fibres and Epoxy Resin Microdroplets." *Composites Science and Technology* 64 (5): 767–72. <https://doi.org/10.1016/j.compscitech.2003.08.002>.
- Erdogan, H., G. Özcebe, and B. Binici. 2007. "A New CFRP Strengthening Technique to Enhance Punching Shear Strength of RC Slab-Column Connections." *Proceedings of the 1st Asia-Pacific Conference on FRP in Structures, APFIS 2007* 1 (Apfis): 233–38.
- Fan, Mizi. 2010. "Characterization and Performance of Elementary Hemp Fibres: Factors Influencing Tensile Strength." *BioResources* 5 (4): 2307–22. <https://doi.org/10.15376/biores.5.4.2307-2322>.
- Genikomsou, Aikaterini. 2018. "Nonlinear Finite Element Analysis of Punching Shear of Reinforced Concrete Slabs Supported on Rectangular Columns," 410. https://uwspace.uwaterloo.ca/bitstream/handle/10012/13631/Milligan_Graeme.pdf?sequence=1.
- Genikomsou, Aikaterini S., and Maria Anna Polak. 2016. "Finite-Element Analysis of Reinforced Concrete Slabs with Punching Shear Reinforcement." *Journal of Structural Engineering* 142 (12): 04016129. [https://doi.org/10.1061/\(asce\)st.1943-541x.0001603](https://doi.org/10.1061/(asce)st.1943-541x.0001603).

- George, Jayamol, M. S. Sreekala, and Sabu Thomas. 2001. "A Review on Interface Modification and Characterization of Natural Fiber Reinforced Plastic Composites." *Polymer Engineering and Science* 41 (9): 1471–85. <https://doi.org/10.1002/pen.10846>.
- Ghalieh, Lea, Elie Awwad, George Saad, Helmi Khatib, and Mounir Mabsout. 2017. "Concrete Columns Wrapped with Hemp Fiber Reinforced Polymer - An Experimental Study." *Procedia Engineering* 200 (December): 440–47. <https://doi.org/10.1016/j.proeng.2017.07.062>.
- Hamoda, A., and K. M.A. Hossain. 2019. "Numerical Assessment of Slab–Column Connection Additionally Reinforced with Steel and CFRP Bars." *Arabian Journal for Science and Engineering* 44 (10): 8181–8204. <https://doi.org/10.1007/s13369-019-03846-2>.
- Harajli, M. H., and K. A. Soudki. 2003. "Shear Strengthening of Interior Slab–Column Connections Using Carbon Fiber-Reinforced Polymer Sheets." *Journal of Composites for Construction* 7 (2): 145–53. [https://doi.org/10.1061/\(asce\)1090-0268\(2003\)7:2\(145\)](https://doi.org/10.1061/(asce)1090-0268(2003)7:2(145)).
- Harajli, M. H., K. A. Soudki, and T. Kudsi. 2006. "Strengthening of Interior Slab–Column Connections Using a Combination of FRP Sheets and Steel Bolts." *Journal of Composites for Construction* 10 (5): 399–409. [https://doi.org/10.1061/\(asce\)1090-0268\(2006\)10:5\(399\)](https://doi.org/10.1061/(asce)1090-0268(2006)10:5(399)).
- Jeeho, Lee, and Fenves Gregory L. 1998. "Plastic-Damage Model for Cyclic Loading of Concrete Structures." *Journal of Engineering Mechanics* 124 (8): 892–900.
- Kabir, M. H., S. Fawzia, T. H.T. Chan, and M. Badawi. 2016. "Numerical Studies on CFRP Strengthened Steel Circular Members under Marine Environment." *Materials*

- and Structures/Materiaux et Constructions 49 (10): 4201–16.
<https://doi.org/10.1617/s11527-015-0781-5>.
- Keller, Nicole M. 2013. “The Legalization of Industrial Hemp and What It Could Mean for Indiana’s Biofuel Industry.” *Indiana International & Comparative Law Review* 23 (3): 555–89. <https://doi.org/10.18060/17887>.
- King, Suzanne, and Norbert J. Delatte. 2004. “Collapse of 2000 Commonwealth Avenue: Punching Shear Case Study.” *Journal of Performance of Constructed Facilities* 18 (1): 54–61. [https://doi.org/10.1061/\(asce\)0887-3828\(2004\)18:1\(54\)](https://doi.org/10.1061/(asce)0887-3828(2004)18:1(54)).
- Lubliner, J, J Oliver, S Oller, and E Onate. 1989. “A Plastic-Damage Model.” *International Journal of Solids and Structures* 25 (3): 299–326.
- Mirzaei.Y, and Sasani.M. 2011. “Structures Congress 2011 © ASCE 2011 2297,” 2297–2308.
- Nishino, T. 2004. “Natural Fiber Sources. In C. Baille, *Green Composites: Polymer Composites and the Environment*.” Woodhead Publishing, no. 1st Edition: 49–80.
<https://doi.org/10.21660/2018.47.STR167>.
- Placet, Vincent. 2009. “Characterization of the Thermo-Mechanical Behaviour of Hemp Fibres Intended for the Manufacturing of High Performance Composites.” *Composites Part A: Applied Science and Manufacturing* 40 (8): 1111–18.
<https://doi.org/10.1016/j.compositesa.2009.04.031>.
- Placet, Vincent, Frédérique Trivaudey, Ousseynou Cisse, Violaine Gucheret-Retel, and M. Lamine Boubakar. 2012. “Diameter Dependence of the Apparent Tensile Modulus of Hemp Fibres: A Morphological, Structural or Ultrastructural Effect?” *Composites Part A: Applied Science and Manufacturing* 43 (2): 275–87.
<https://doi.org/10.1016/j.compositesa.2011.10.019>.

- R. D. MOWRER and M. D. VANDERBILT. 1967. "Shear Strength of Lightweight Aggregate Reinforced Concrete Flat Plates." *ACI Journal Proceedings* 64 (11): 722–29. <https://doi.org/10.14359/7601>.
- Rahman Khan, Md Majibur, Ying Chen, Tamara Belsham, Claude Laguë, Hubert Landry, Qingjin Peng, and Wen Zhong. 2011. "Fineness and Tensile Properties of Hemp (*Cannabis Sativa L.*) Fibres." *Biosystems Engineering* 108 (1): 9–17. <https://doi.org/10.1016/j.biosystemseng.2010.10.004>.
- Sen, Tara, and H. N. Jagannatha Reddy. 2013. "Strengthening of RC Beams in Flexure Using Natural Jute Fibre Textile Reinforced Composite System and Its Comparative Study with CFRP and GFRP Strengthening Systems." *International Journal of Sustainable Built Environment* 2 (1): 41–55. <https://doi.org/10.1016/j.ijse.2013.11.001>.
- Sen, Tara, and Ashim Paul. 2015. "Confining Concrete with Sisal and Jute FRP as Alternatives for CFRP and GFRP." *International Journal of Sustainable Built Environment* 4 (2): 248–64. <https://doi.org/10.1016/j.ijse.2015.04.001>.
- Sen, Tara, and H. N. Jagannatha Reddy. 2014. "Flexural Strengthening of RC Beams Using Natural Sisal and Artificial Carbon and Glass Fabric Reinforced Composite System." *Sustainable Cities and Society* 10: 195–206. <https://doi.org/10.1016/j.scs.2013.09.003>.
- Shahzad, Asim. 2012. "Hemp Fiber and Its Composites - A Review." *Journal of Composite Materials* 46 (8): 973–86. <https://doi.org/10.1177/0021998311413623>.
- Sharaf, Mohamed H., Khaled A. Soudki, and Michael Van Dusen. 2006. "CFRP Strengthening for Punching Shear of Interior Slab–Column Connections." *Journal of Composites for Construction* 10 (5): 410–18. [https://doi.org/10.1061/\(asce\)1090-](https://doi.org/10.1061/(asce)1090-)

0268(2006)10:5(410).

- Silva, M. A.L., J. C.P.H. Gamage, and S. Fawzia. 2019. "Performance of Slab-Column Connections of Flat Slabs Strengthened with Carbon Fiber Reinforced Polymers." *Case Studies in Construction Materials* 11: e00275. <https://doi.org/10.1016/j.cscm.2019.e00275>.
- Smith, Michael. 2009. "ABAQUS/Standard User's Manual, Version 6.9/." Dassault Systèmes Simulia Corp, Providence, RI.
- Soudki, Khaled, Ahmed K. El-Sayed, and Tim Vanzwol. 2012. "Strengthening of Concrete Slab-Column Connections Using CFRP Strips." *Journal of King Saud University - Engineering Sciences* 24 (1): 25–33. <https://doi.org/10.1016/j.jksues.2011.07.001>.
- Wang, Hongguang, and Guijun Xian. 2020. "Shear Capacity of RC Beams Strengthened with Flax Fiber Sheets Grafted with Nano-TiO₂." *Materials* 13 (6): 1–20. <https://doi.org/10.3390/ma13061430>.
- Yinh, Seyha, Qudeer Hussain, Winyu Rattanapitikon, and Amorn Pimanmas. 2016. "Flexural Behavior of Reinforced-Concrete (RC) Beams Strengthened with Hemp Fiber-Reinforced Polymer (FRP) Composites." *Materials Science Forum* 860: 156–59. <https://doi.org/10.4028/www.scientific.net/MSF.860.156>.

